Title

Generate a new crucian carp (*Carassius auratus*) strain without intermuscular bones by knocking out *bmp6*

Youyi Kuang[1,2,3,4,*], Xianhu Zheng[1,2,3], Dingchen Cao[1,2,3], Zhipeng Sun[1,2,3], Guangxiang Tong[1,2,3], Huan Xu[1,2,3], Ting Yan[1,2,3], Shizhan Tang[1,2,3], Zhongxiang Chen[1,2,3], Tingting Zhang[1,2,3], Tan Zhang[1,2,3], Le Dong[1,2,3], Xiaoxing Yang[1,2,3], Huijie Zhou[1,2,3], Weilun Guo[1,2,3], Xiaowen Sun[1,2,3,*]

Affiliation

1. National and Local Joint Engineering Laboratory for Freshwater Fish Breeding, No. 232, Hesong Street, Daoli District, Harbin 150070, China
2. Key Laboratory of Freshwater Aquatic Biotechnology and Breeding, Ministry of Agriculture and Rural Affairs, No. 232, Hesong Street, Daoli District, Harbin 150070, China
3. Heilongjiang River Fisheries Research Institute of Chinese Academy of Fishery Sciences, No. 232, Hesong Street, Daoli District, Harbin 150070, China
4. Heilongjiang Provincial Key Laboratory of Hard Tissue Development and Regeneration, The Second Affiliated Hospital of Harbin Medical University, Harbin 150081, China

E-Mail:

Youyi Kuang: kuangyouyi@hrfri.ac.cn
Xianhu Zheng: zhengxianhu@hrfri.ac.cn
Dingchen Cao: caodingchen@hrfri.ac.cn
Zhipeng Sun: sunzhipeng@hrfri.ac.cn
Guangxiang Tong: tongguangxiang@hrfri.ac.cn
Huan Xu: xuhuan@hrfri.ac.cn
Ting Yan: yanting@hrfri.ac.cn
Shizhan Tang: tsz2007@163.com
Zhongxiang Chen: chenzx@hrfri.ac.cn
Tingting Zhang: 1260242608@qq.com
Tan Zhang: tan_zhg@sina.com
Le Dong: 610478772@qq.com
Xiaoxing Yang: 1393072122@qq.com
Huijie Zhou: 1668312678@qq.com
Weilun Guo: 1172141357@qq.com
Xiaowen Sun: sunxw2002@163.com

* To whom correspondence should be addressed.
Youyi kuang, E-Mail: kuangyouyi@hrfri.ac.cn; Tel: +86-451-87930951; Xiaowen Sun, E-Mail: sunxw2002@163.com；Tel:+86-451-84842646

Abstract

Elimination of intermuscular bones (IMBs) is vital to the aquaculture industry of cyprinids. In our previous study, we characterized *bmp6* as essential in the development of IMBs in zebrafish. Knockout of *bmp6* results in the absence of IMBs in zebrafish without affecting growth and reproduction. Therefore, we hypothesized that *bmp6* could be used to generate new cyprinid strains without IMBs by gene editing. In this study, we established a gene editing strategy for knocking out the two orthologs of *bmp6* in diploid crucian carp (*Carassius auratus*). We obtained an F_3 population with both orthologs knocked out, in which no IMBs were detected by bone staining and X-ray, indicating that the new strain without IMBs (named WUCI strain) was successfully generated. Furthermore, we extensively evaluated the performance of the new strain in growth, reproduction, nutrient components, muscle texture and structure, and metabolites in muscle. The results showed that the WUCI strain grew faster than the wild-type crucian carp at 4-month-age. The reproductive performance and flesh quality did not show significant differences between the WUCI strain and wild-type crucian carp. Moreover, the metabolomics analysis suggested that the muscle tissues of the WUCI strain significantly enriched some metabolites belonging to the Thiamine metabolism, Nicotinate and Nicotinamide Metabolism pathway, which plays beneficial effects in anti-aging, anti-oxidant, and anti-radiation damage. In conclusion, we established a strategy to eliminate IMBs in crucian carp and obtain a WUCI strain whose performance was expected compared to the wild-type crucian carp; meanwhile, the WUCI strain enriched some beneficial metabolites to human health in muscle tissue. This study is the first report that a farmed cyprinid strain without IMBs, which could be stably inherited, was obtained worldwide; it provided excellent germplasm for the cyprinids aquaculture industry and a useful molecular tool for eliminating IMBs in other cyprinids.

Keywords: crucian carp, a new strain without intermuscular bones, *bmp6*, gene editing, performance evaluation

1. Introduction

Cyprinids are the most important aquaculture species in China, with an annual production of about 27 million tons, occupying around 76% of total freshwater fish aquaculture production. However, the intermuscular bones (hereafter IMBs) severely cause food inconvenience and may even lead to physical injuries such as being stuck in the throat. The processing of fish products (such as fish balls) is also hindered. The genetic breeding of eliminating IMBs of cyprinids has become an increasing interest in China(Gui et al., 2021; Nie et al., 2020; Sun and Zhu, 2019).

The genetic breeding of strains without IMBs in cyprinids began in the 1960s (Meske, 1968) , but there has been no progress until the last decade. With the development of biotechnology, some progress has been made in the genetic breeding of IMBs. For example, Xu et al. (2015) found a mutant with normal growth and absence of IMBs from a gynogenesis population of grass carp(*Ctenopharyngodon idellus*); Peruse et al.(2017) obtained a population with IMBs deficient in *Colossoma macropomum* by X-ray scan; Wu et al. (2020) obtained a population with a 5.7% reduction in the count of IMBs by crossing *Megalobrama amblycephala* and *Culter alburnus*, indicating that varieties with less count of IMBs can be obtained by crossbreeding. Lin et al.(2013) reported that hybrid crucian carp (*Carassius auratus*) had a smaller number of IMBs than wild crucian carp, and the count of IMBs of crucian carp could be reduced by polyploid breeding and crossbreeding methods; Cao et al. (2015) concluded that mirror carp (*Cyprinus carpio*) could be an excellent candidate for genetic selection to reduce IMBs. In terms of genetic and molecular breeding, Xiong et al. (2019) found that the heritability of the number of IMBs differed in different parts of blunt snout bream (*M. amblycephala*); Wan et al. (2019) identified single nucleotide polymorphism (SNP) markers associated with the count of IMBs in *M. amblycephala*. The counts of IMBs were significantly different among common carp (*C. carpio*) species/strains and families (Cao et al., 2015; Tang et al., 2020). However, the heritability of IMBs was low, with a value of 0.15 (Tang et al., 2020) . Eight significant QTL intervals were obtained in the QTL analysis of the number of IMBs in mirror carp, which explained 7.7-25.9% of the phenotypic variation(Tang et al., 2020).

From the above statements, it is clear that genetic improvement of IMBs can be carried out by artificial selection, cross breeding, gynogenesis, polyploid breeding, and molecular marker-assisted selection; however, there is still no breakthrough in reducing more than 50% of IMBs. With the development of gene editing technology, the genes and regulatory elements affecting the development of IMBs have been characterized. For example, Nie et al. (2021) knocked out *scxa* in zebrafish and obtained a mutant with more than 70% reduction in the count of IMBs, rib hypoplasia, and defective septal development(Kague et al., 2019; Nie et al., 2021). In our previous study, we characterized that *bmp6* regulates the development of IMBs in zebrafish(Xu et al., 2022) , and its knockout causes the complete absence of IMBs in zebrafish without affecting the growth, muscle, and bone development of zebrafish (Jian et al., 2019; Xu et al., 2022; Yang et al., 2021, 2020). Therefore, we hypothesize that *bmp6* could be used to generate new cyprinid strains without IMBs by gene editing.

In this study, we generated a new crucian carp (*C. auratus*) strain without IMBs (hereafter WUCI strain) by knocking out *bmp6* and demonstrated that knockdown of *bmp6* did not affect the growth, and nutritional quality of the strain; we also conducted a metabolomics analysis of muscle to explore the effects of *bmp6* on substance synthesis and metabolism. This study provided an excellent germplasm for

the cyprinids aquaculture industry and a useful molecular tool for eliminating IMBs in other cyprinids.

2. Materials and methods

2.1 Experimental fish

The diploid crucian carp (*C. auratus*, 2n=100) used in this study were cultured in the Hulan Experimental Station of HRFRI. Parental fish were reared in a 700m^2 pond and injected with oxytocin drugs, including luteinizing hormone-releasing hormone (LRH-2, 4ug/kg body weight); domperidone (DOM, 1mg/kg body weight), and human chorionic gonadotropin (HCG, 100 U/kg body weight) for spawning. The fertilized eggs were incubated in 24cm×20cm×24cm incubation tanks at 22℃～23℃. After hatching, larvae were fed 4 times/day of Artemia until they grew up to 2cm-3cm in body length; the larvae were moved to a 500m^2 pond and fed artificial feed 2 times/day. The rear condition of F_0, F_1, F_2, and F_3 generation in the present study was the same as the above description.

2.2 *Bmp6* knockout

Because the crucian carp underwent the fourth round of genome duplication event(Chen et al., 2019), there are two orthologs of *bmp6* in the crucian carp genome. To identify the two orthologs, the cDNA and protein sequence of zebrafish *bmp6* were aligned to the crucian carp genome (Chen et al., 2019) using Blast tools, and the two orthologs were validated by the annotation of Ensembl(http://www.ensembl.org), which were ENSCARG00000018439(*bmp6a*) and ENSCARG00000056616(*bmp6b*).

The *bmp6a* and *bmp6b* knockout were carried out according to the method described by Xu et al. (2022) and described as follows. The target sites for CRISPR/Cas9 knockout were designed using the CHOPCHOP service (Labun et al., 2019) (Supplementary Table S1). The sgRNA was synthesized using the NEB HiScribe T7 Fast and Efficient RNA Synthesis Kit (NEB E2050S, MA, USA). After mixing 5μM~10μM sgRNAs of *bmp6a* and *bmp6b* and 5μM Cas9 protein (M0646, NEB, MA, USA), 1nL mixture was micro-injected into single-cell embryos. The embryos were incubated at 22~23℃ as described above.

2.3 Mutants screening

After four months of culture, fish were labeled with PIT tags, and fin clips were collected for DNA extraction. The fin clips were lysed with 100μl solution consisting of 0.5 mg/ml proteinase K, 10 mmol/L pH 8.0 1 M Tris, 50 mmol/L KCl, 0.3% Tween 20, 0.3% NP 40 at 55°C for 6 h and 98°C for 10 min. After lysis, the lysate was mixed and centrifuged at 1000-2000 rpm for 2 min, and the supernatant was taken for PCR amplification.

The method for screening mutants is illustrated in Fig. 2(c). In this procedure, PCR amplification was performed using the method described by Tong et al. (2018) and was briefly described as follows. Two pairs of primers were used for PCR amplification, one of which was the target primer for amplifying the target fragment (Supplementary Table S2), and the other was the index primer for indexing samples. A 2-step amplification was performed: firstly, the PCR was carried out using 10μL volume, including genomic DNA supernatant 1μL, 1μmol/L forward and reverse

target primers 0.5μL, 2× Dream Taq Master Mix (Thermo Fisher, CA, USA) 5μL, the PCR was performed with 95°C for 3 min, followed by 10cycles of 95°C 30 s, 60°C 30 s, 72°C 30 s; 72°C for 2 min; the second PCR amplification was performed by adding 0.5μL of 5μmol/L forward and reverse index primers to the first step PCR product, and the PCR program was set to 95°C for 2 min; 6 cycles of 95°C 30 s, 58°C 30 s, 72°C 30 s; and 15 cycles of 95°C 30 s, 72°C 30s, finally 72°C 2min.

After PCR amplification, PCR products were mixed in equal amounts, DNA sequencing libraries were constructed using the TrueSeq library prepare kit, and 300bp Pair-End sequencing was performed using the Illumina MiSeq sequencing platform. The data obtained by MiSeq were first used to identify the loci and samples with the method described by Tong et al. (2018) , followed by analysis with CRISPResso2 (Fiume et al., 2019) to screen the mutants and calculate the somatic mutation rate of each sample.

2.4 Intermuscular bone observation

We used skeleton staining, X-ray, and micro-CT to observe IMBs. Skeleton was stained using Alizarin red with the method described by Yang et al. (2020) and observed using the Zeiss Stereo Discovery V8 system (Carl Zeiss, Jena, Germany), the X-ray observation was performed using Faxitron MX-20 X-ray System(Faxitron, MA, USA), and the Quantum GX micro-CT Imaging System (PerkinElmer, MA, USA) with 70 KV, 88μA, and 14 min scan time was used for micro-CT. Around 50dph~60dph fish were used for bone staining, and four-month-old fish was used for X-ray and micro-CT scan. The counts of IMBs were checked using the images from bone staining and the X-ray.

2.5 Growth and reproductive performance evaluation

After one month of culture in a pond, 600 fingerlings of WUCI strain with BW of 4.6±0.42g and 600 fingerlings of wild-type crucian carp with BW of 4.2±0.55g were raised in a 500m^2 pond. During the culture, the SL and BW were measured each month. At the age of 4 months, 50 individuals of WUCI strain and wild-type crucian carp were randomly chosen to measure the BW and SL. Furthermore, the gonad of 30 individuals from each group was dissected for weighting and histological examination according to Gan et al. (2021) . The absolute fecundity and relative fecundity were calculated with the method described by Franěk et al.(2021).

2.6 Flesh quality evaluation

Thirty 4-month-old fish from each group were selected to evaluate flesh quality. For the texture analysis, the dorsal muscle with a size of 1cm^3 and 2cm*1cm*1cm was dissected to measure the hardness, cohesiveness, springiness, gumminess, chewiness, and shear force using a TMS-Pro texture meter (Food Technology Corporation, VA, USA). The remained muscle tissues were dissected to measure the nutrient components, and muscles from 10 individuals were pooled; 3 pooled samples of each group were tested. Moreover, the content of trace elements was measured using dorsal muscle and liver tissues from 5 fish of each group. Additionally, dorsal muscles from 5 fish of each group were dissected for histological analysis according to Yang et al.(2021).

The nutrient components, including proximate compositions (moisture, crude ash, crude protein, and crude lipid), amino acid compositions, fatty acid compositions, and vitamin compositions (A, B1, B2, D, and E) were measured in Qingdao Sci-tech Innovation Quality Testing Co., Ltd. according to the national standards of China. The

contents of trace elements, including Mg, Mn, Fe, Zn, Cu, Se, and K, were measured using inductively coupled plasma-mass spectrometry (ICP-MS, Agilent 7500cx, USA).

2.7 RT-qPCR of *bmp6a* and *bmp6b*

Ten organs, including intestine, liver, dorsal muscle, caudal muscle, brain, spleen, skin, gill, kidney, and heart from 6 wild-type crucian carp at 4-month-age were dissected for total RNA extraction using Trizol (Thermo Fisher, CA, USA). RNA quality was measured using Nanodrop 8000 (Thermo Fisher, CA, USA), and the quantity of RNA was measured using the Qubit3 kit (Thermo Fisher, CA, USA). The RNA was reverse-transcribed with the Revert Aid^{TM} First-Strand cDNA Synthesis Kit (Thermo Fisher, CA, USA). The qPCR was analyzed with primers listed in Supplementary Table S3, and *β-actin* was used as the reference gene (Dharmaratnam et al., 2021). The RT-qPCR was carried out using 10 μL volume, including 1 μL of 50ng/μL cDNA, 0.5μL of 10μM forward and reverse primer, 5μL of 2× Luna Universal qPCR Master Mix (NEB, MA, USA). The amplification program was set as follows: 95℃ for 15s, followed by 40 cycles of 95℃ 15s and 60℃ for 30s. The qPCR was performed using the QuantiStudio 6 Flex Real-Time PCR System (Thermo Fisher, CA, USA).

2.8 RNA fluorescence in situ hybridization

We used the caudal muscle tissues of 60dph wild-type crucian carp to detect the spatial expression of *bmp6a* and *bmp6b*. The RNA fluorescence in situ hybridization was carried out with the SABER-FISH protocol according to Kishi et al.(2019, 2018). The probes were designed by the method proposed by Beliveau et al. (Beliveau et al., 2018) and listed in Supplementary Table S4. the mRNA of *bmp6a* and *bmp6b* was detected using Alexa Fluor 532 probes, and the nucleus was stained using DAPI dye (Thermo Fisher, CA, USA). The cryosections were observed using a fluorescence microscope (OLYMPUS BX53, Japan), and the images were processed by ImageJ.

2.9 Metabolomics analysis

The dorsal muscle tissues of 15 fish from each group were dissected and frozen in liquid nitrogen for metabolomics analysis. The tissues were grounded with liquid nitrogen, and after resuspending with prechilled 80% methanol by vortex, the samples were incubated on ice for 5min and were centrifuged for 20min at 15000g and 4°C; the supernatants were diluted to a final concentration of 53% methanol by LC-MS grade water and transferred to fresh Eppendorf tubes. After centrifugation at 15000g and 4°C for 20min, the supernatant was subjected to the LC-MS/MS system. The UHPLC-MS/MS analyses were carried out using a Vanquish UHPLC system (Thermo Fisher, Germany) coupled with an Orbitrap Q Exactive HF-X mass spectrometer (Thermo Fisher, Germany) in Novogene Co., Ltd. (Bejing, China).

The original file obtained by UHPLC-MS/MS was imported into Compound Discoverer 3.1 (CD3.1) software for s pectrogram processing with parameters of retention time tolerance of 0.2 min, an actual mass tolerance of 5ppm, signal intensity tolerance of 30%, and signal/noise ration of 3. After normalization to the total spectral intensity, the normalized peak intensities were used to predict the molecular formula based on additive ions, molecular ion peaks, and fragment ions. The databases of mzCloud(https://www.mzcloud.org), mzVault, and MassList database were used to match the peak and obtain accurate qualitative and relative quantitative results.

The quantitative matrix of metabolites was analyzed by multivariate statistical

analysis, including principal component analysis (PCA) and partial least squares discriminant analysis (PLS-DA) to reveal the differences in metabolic patterns among different groups. The univariate analysis (Student's t-test) was used to calculate the statistical significance, the metabolites with P-values<0.05, variable importance in the projection (VIP) value >1.0, and fold-change(FC) of WUCI vs. wild-type ≥1.5 or ≤0.667 were considered to differential metabolites. After annotating with KEGG, HMDB (https://hmdb.ca/metabolites), and LIPIDMaps database (http://www.lipidmaps.org), pathway analysis was carried out using MetaboAnalyst 5.0(Pang et al., 2022)

2.10 Statistical analysis

Student's t-test was used to test the significance of the difference in body length, body weight, and muscle texture structure. And Wilcoxon Rank Sum Test was used to test the significance of the difference in reproductive performance, results of histological analysis, and content of elements and nutrients.

3. Results

3.1 Expression pattern of duplicated *bmp6* in crucian carp

Bmp6 has been indicated to co-express in the myoseptum with osteoblast marker gene *sp7*, tendon progenitor marker gene *scxa,* and tenocyte marker gene *tnmd* and *xirp2a* (Xu et al., 2022) . However, *bmp6* had two orthologs (*bmp6a*: ENSCARG00000018439; *bmp6b*: ENSCARG00000056616) in the crucian carp genome caused by the fourth whole-genome duplication event (Fig. 1(a))(Chen et al., 2019) . To explore whether the two duplicated copies had a similar function to the development of IMBs in crucian carp, we investigated the expression levels in 9 tissues using RT-qPCR; *bmp6a* had a high expression level in dorsal muscle, caudal muscle, and skin; *bmp6b* had a high expression level in liver and gill (Fig. 1(a), (c)); Supplementary Figs. S1, S2). The spatial expression of *bmp6a* and *bmp6b* in caudal muscle detected by RNA fluorescence in situ hybridization (RNA-FISH) showed that both orthologs were expressed in the myoseptum(Fig. 1(d-e); Supplementary Fig. S3). These results indicated that both orthologs might function in IMB's development despite the expressed levels.

3.2 Pipeline for *bmp6* gene editing in crucian carp

According to the expression in muscle, *bmp6a* and *bmp6b* should be knocked out simultaneously to obtain individuals without IMBs. In order to rapidly establish the WUCI strain, we designed a two-round gene knockout and mating strategy in this study (Fig. 2(a)). In this strategy, three target sites were designed in exon 1 of *bmp6a* and *bmp6b*, respectively (Fig. 2(b)). Firstly, sgRNAs of *bmp6a* and *bmp6b* were used for the first round of multiplex gene knockout to construct the F_0 generation, and the mutants of F_0 generation were screened by high-throughput sequencing using PCR products of target sites (Fig. 2(c)). The mutants with somatic mutation rates of more than 95% (*bmp6a* or *bmp6b*) were selected for natural mating, and the second round of multiplex gene knockout of *bmp6a* and *bmp6b* was performed in their fertilized eggs to construct the F_1 generation. In the F_1 generation, individuals with somatic mutation rates of more than 95% *bmp6a* and *bmp6b* were scanned by X-ray to screen

individuals without IMBs, which were used to construct the F_2 generation population by self-bred. Genotypes and counts of IMBs of the F_2 generation were screened, and individuals without IMBs were used for reproducing the F_3 generation by self-bred. Individuals of the F_3 generation were used for evaluating the growth and fecundity performance, nutrient components, and metabolomics analysis.

3.3 Generation of a new strain without intermuscular bones

Using this pipeline, we carried out *bmp6* gene editing in crucian carp and generated the WUCI strain from 2019 to 2022(Fig. 3(a)). Among 668 F_0 progenies, 511 mutants were screened, including 117 mutants with *bmp6a* and *bmp6b* mutated in somatic cells (Fig. 3(b) Supplementary Table S5). The somatic mutation rate of *bmp6a* and *bmp6b* in F_0 mutants were 52.20%~96.10% and 20.80~99.80, respectively (Fig. 3(b), Supplementary Table S6), with the mean value of 72.1% and 75.74%, respectively. The percent of mutants with somatic mutation ratio ⩾95% of *bmp6a* and *bmp6b* was 0.61% and 27.1%, respectively.

After the knockout of *bmp6a* and *bmp6b* for the second time using F_0 adults, 1130 F_1 progenies were obtained, among which 947 mutants were screened, including 630 mutants with *bmp6a* and *bmp6b* mutated in somatic cells (Fig. 3(b), Supplementary Table S5). The somatic mutation rate of *bmp6a* and *bmp6b* in F_1 mutants were 61.70%~100% and 36.70%~100%, respectively (Fig. 3(b), Supplementary Table S6), with the mean value of 93.4% and 97.25%, respectively. The percent of mutants with somatic mutation ratio ⩾95% of *bmp6a* and *bmp6b* was 64.65% and 89.58%, respectively.

A comparative analysis showed that the somatic mutation rates of *bmp6a* or *bmp6b* in the F_1 mutants were significantly higher than those in the F_0 mutants ($P<0.0001$, Fig. 3(b), Supplementary Table S5). The number of mutants with both genes mutated and the number of mutants with a somatic mutation rate of more than 95% in the F_1 generation was also significantly higher than those in the F_0 generation ($P<0.0001$, Fig. 3(c), Supplementary Table S6), and the somatic mutation rate of samples with both genes mutated in F_1 mutants was also significantly higher than in F_0 mutants ($P<0.0001$, Fig. 3(c), Supplementary Table S6). These results indicated that the two-round gene knockout strategy significantly increased the mutation rate and the number of samples with high mutation rates of both genes, resulting in the rapid establishment of homozygous mutated lines.

The in-frame and frameshift mutation rates of *bmp6a* and *bmp6b* in the F_0 and F_1 mutants were listed in Supplementary Table S6. The number of in-frame mutation of *bmp6a* in the F_0 mutants were significantly higher than those in the F_1 mutants, and the number of in-frame mutation of *bmp6b* in the F_1 mutants were significantly higher than those in the F_0 mutants ($P<0.0001$, Fig. 3(d)). The number of frame-shift mutation of *bmp6a* in the F_1 mutants were significantly higher than those in the F_0 mutants, and the number of frame-shift mutation of *bmp6b* in the F_0 mutants were significantly higher than those in the F_1 mutants ($P<0.0001$, Fig. 3(e)).

In the F_1 generation, 270 progenies with 95% somatic mutation rate of *bmp6a* and *bmp6b* were screened, among which 35 mutants without IMBs were obtained using X-ray scanning (Fig. 3(f)), accounting for 12.96%; additionally, 110 mutants with more than 50% reduction of the count of IMBs were screened, accounting for 40.74%. The F_2 population was constructed using the 35 F_1 mutants without IMBs at one year old by self-bred; among 1500 F_2 progenies, 285 individuals without IMBs were obtained, accounting for 19.00%, and 380 individuals with the count of IMBs reduced by more than 50%, accounting for 25.33% (Fig. 3(g)). Furthermore, sexually

matured individuals without IMBs of the F_2 generation at one year old were used to construct the F_3 generation population by self-bred, and 41 individuals at 60dph (days post-hatched) were randomly chosen for bone staining, no IMB was found in staining (Fig. 3(h)). We also examined the IMBs by X-ray using 30 individuals at 4 months of age and approved the results (Fig. 3(i)). These results indicated that the WUCI strain was generated successfully.

The genotype analysis of F_1, F_2, and F_3 generation showed that the WUCI strain was a multiple mutated alleles population. We randomly chose five individuals from 35 F_1 mutants without IMBs to sequence the target site of *bmp6a* and *bmp6b,* and the results showed that 21 mutated alleles in somatic cells were observed in *bmp6a* (Supplementary Fig. S4-S5) and 11 mutated alleles in somatic cells were observed in *bmp6b* (Supplementary Fig. S6-S7), a frame-shift mutation occurred at the around 23rd amino acid of *bmp6a* and *bmp6b*(Supplementary Fig. S5, S7). The genotypes of F_2 individuals without IMBs (bottom right in Fig. 3(g)) used for constructing the F_3 generation showed that 9 mutated alleles were observed in *bmp6a* and 5 mutated alleles were observed in *bmp6b*(Supplementary Figure S8), all the mutation caused frame-shift at the around 23rd amino acid in *bmp6a* and the around 22nd amino acid of *bmp6b*. Additionally, we carried out the knockout of a single gene (*bmp6a* or *bmp6b*) and checked the genotypes (Supplementary Figure S9) and phenotypes of the homozygous lines ($bmp6a^{-/-}$;$bmp6b^{+/+}$ at the top right of Fig. 3(g) and $bmp6a^{+/+}$;$bmp6b^{-/-}$ at the bottom left of Fig. 3(g)), the results showed that the knockout of *bmp6a* or *bmp6b* caused the partial deletion of IMBs in homozygous mutants (top right and bottom left in Fig. 3(g)). We also randomly genotyped 5 individuals of the F_3 generation and observed 5 mutated alleles in *bmp6a* and 4 mutated alleles in *bmp6b*, which were inherited from the F_2 parents (Supplementary Fig. S10).

3.4 Growth of the new strain

For evaluating the growth performance of the WUCI strain, 600 one-month-old fingerlings of WUCI strain with body weight (BW) around 4.6±0.42g and body length(SL) around 4.94±0.38mm and 600 one-month-old fingerlings of wild-type crucian carp with BW around 4.2±0.55g and SL approximately 4.79±0.35mm were cultured for three months at a 500m^2 pond, the BW and SL were measured each month. The relationship between BW and SL of the WUCI strain was similar to that of the wild-type crucian carp (Supplementary Fig. S11). The comparisons showed that the SL and increment of SL per month of the WUCI strain were significantly higher than that of wild-type crucian carp at 2, 3, and 4 months of age(Fig. 4(a-b), Supplementary Table S7); there was no significant difference in specific growth rate(SGR) of SL per month between the WUCI strain and wild-type crucian carp at 2,3months of age, whereas, a significant difference(P<0.001) in SGR of SL at four months of age was observed(Fig. 4(c), Supplementary Table S7). The growth of BW was similar to that of SL (Fig. 4(d-f), Supplementary Table S7). Based on the above analysis results, it can be concluded that the WUCI strain at 2~4-month-old grew faster than the wild-type crucian carp.

3.5 Nutrient components of the new strain

The nutrient components in muscle tissue of 4-month-old WUCI strain and wild-type crucian carp were determined. We analyzed the proximate composition, total saccharide, vitamins, fatty acids, and amino acids (Supplementary Table S8-11). Seventeen kinds of amino acids and 17 types of fatty acids were determined. Among the five vitamins (A, B1, B2, D, and E) we measured, vitamins A and D were not

detected. The comparison results showed that there was no significant difference in the contents of nutrient components mentioned above, as well as essential amino acid (EAA), umami amino acid (UAA), essential fatty acid (EFA), polyunsaturated fatty acid (PUFA), Omega3, and Omega6 (Fig. 5, Supplementary Table S8-11). We also measured seven elements in the muscle and liver tissues, including Mg, Mn, Fe, Cu, Zn, Se, and K. The significance test showed that the contents of Fe and Se in the liver of the WUCI strain were significantly higher than those of the wild-type crucian carp. In contrast, the contents of all elements in the muscle did not show a significant difference (Fig. 6, Supplementary Table S12).

3.6 Muscle texture and structure of the new strain

Muscle texture and structure are important to fish flesh quality. The muscle texture analysis showed that the shear force of the WUCI strain was significantly higher than those of wild-type crucian carp($P<0.01$) (Fig. 7(a), Supplementary Table S13). In contrast, the hardness of the WUCI strain was significantly weaker than those of wild-type crucian carp($P<0.05$) (Fig. 7(b), Supplementary Table S13). Furthermore, the two groups had no significant difference in cohesiveness, springiness, gumminess, and chewiness (Fig. 7(c-f), Supplementary Table S13). The PCA analysis result of muscle texture showed that most samples of the WUCI strain were clustered together with those of the wild-type strain and not well distinguished (Supplementary Fig. S12), indicating that no significant difference occurred between the two groups. We also carried out a histological analysis of muscle tissues, and the results showed that the muscle fiber area and density had no significant differences ($P>0.05$) between the WUCI strain and the wild-type crucian carp (Fig. 7(g-i), Supplementary Table S13). These results indicated that the knockout of *bmp6a* and *bmp6b* and the lack of IMBs did not significantly change the muscle texture and structure of the WUCI strain.

3.7 Reproductive performance of the new strain

The comparison analyses showed no significant difference in the weight of ovary and ovarian GSI (Gonadosomatic index, gonad weight/body weight ×100) between the 4-month-old WUCI strain and wild-type crucian carp($P>0.05$) (Fig. 8(a-b); Supplementary Table S14). The weight of the testis and GSI of the WUCI strain were significantly higher than those of wild-type crucian carp ($P<0.01$ and $P<0.05$, respectively) (Fig. 8(a-b); Supplementary Table S14). Moreover, no significant difference between the two groups was observed in the absolute female fecundity (total quantity of produced eggs by females) and relative fecundity (the number of eggs per gram of body weight) ($P>0.05$) (Fig. 8(c-d); Supplementary Table S14). The gonad histological analysis showed that the development of the ovary and testis of the WUCI strain was similar to that of the wild-type crucian carp (Fig. 8(e-f)). These results suggested that the *bmp6a* and *bmp6b* knockout and the absence of IMBs did not significantly affect the gonad development and the fecundity of the WUCI strain.

3.8 Metabolome analysis

The peaks extracted from all samples and QC were analyzed by PCA, and the results showed that the QC samples in the positive and negative ion modes were clustered together (Fig. 9(a-b)), indicating that the experiment was robust. The PLS-DA model of two groups was established, and 7-fold cross-validation was performed to characterize the model's stability and reliability (Fig. 9(c-d)). A total of 863 metabolic ion peaks were extracted, including 546 positive ion peaks and 317

negative ion peaks. Using the parameters of VIP > 1.0, FC > 1.5 or FC < 0.667, and P-value< 0.05, 107 metabolites in the positive ion mode had significant differences, including 28 up-regulated and 79 down-regulated metabolites in the WUCI strain (Supplementary Table S15); in the negative ion mode, 124 metabolites had significant differences, including 5 up-regulated and 119 down-regulated metabolites in the WUCI strain (Supplementary Table S16). These up-regulated metabolites included some metabolites that are beneficial to the organism, such as β-Nicotinamide mononucleotide, DL-Glutamine, Hypoxanthine, Traumatic acid, Thiamine pyrophosphate, and so on (Fig. 9(e-l)). KEGG pathway enrichment analysis showed that 46 metabolite pathways were enriched, including Thiamine metabolism, Glutathione Metabolism, Nicotinate and Nicotinamide Metabolism, amino acids metabolism pathways, etc. (Fig. 9(m), Supplementary Table S17, Supplementary Fig. S13).

4. Discussion

The cyprinids aquaculture industry requires varieties with high flesh quality, and the reduction of IMBs is one of the main targets for improving the flesh quality (Gjedrem, 1997; Gui et al., 2021; Sun and Zhu, 2019). Although researchers utilized many approaches to deplete cyprinids IMBs, little progress was obtained until the eruption of the gene editing technology. In our previous study(Xu et al., 2022), we characterized *bmp6* as an essential gene to the development of IMBs in zebrafish and obtained a zebrafish strain with IMBs completely absent by knockout *bmp6*, in this study, we generated a new strain without IMBs by knocking out the two orthologs, *bmp6a* and *bmp6b.* This strain has expected performances of growth, reproduction, nutrient value, and muscle texture and structure; significantly, its muscle enriched some beneficial metabolites for human health. According to our knowledge, it is the first report that a farmed cyprinid strain without IMBs, which could be stably inherited, was obtained in the world.

There are two orthologs of *bmp6* in crucian carp; according to the expression in the muscles, it is supposed that the two orthologs should be knocked out simultaneously to obtain mutants with complete depletion of IMBs. To test this hypothesis, we generated two additional homozygous lines by knocking out a single gene, *bmp6a* or *bmp6b*, the phenotypes of homozygous mutants of *bmp6a*$^{-/-}$ or *bmp6b*$^{-/-}$ showed that the knockout of *bmp6a* or *bmp6b* caused the partial deletion of IMBs in mutants, whereas the double knockout of *bmp6a* and *bmp6b* caused the complete elimination of IMBs in the F_2 generation which also approved by the phenotypes of the F_3 generation because the F_3 generation was established by self-bred with *bmp6a*$^{-/-}$;*bmp6b*$^{-/-}$ F_2 adults.

In general, multiplex gene knockout homozygous strains were obtained by sequential knocking out a single gene or crossing with homozygous lines with a single gene knockout, which is difficult and time-consuming (around 3~4 generations to get a homozygous line). We established a two-round knockout strategy to obtain homozygous mutants with the simultaneous knockout of *bmp6a* and *bmp6b*. This strategy contains three aspects: firstly, we used three guides to knock out *bmp6a* or *bmp6b*. Wu et al. (2018) proved that the simultaneous use of multiple guides could significantly increase the efficiency of functional disruption; we adopted this strategy and obtained mutants in more than 70% of the F_0 generation (Supplementary Table S5, S6). Secondly, the mutants with more than 95% mutation rate of somatic cells were chosen to reproduce the next generation. Generally, the mutation in germ cells was unknown, and we supposed that the gene in germ cells should be mutated if the

523 somatic mutation rate was more than 95%, if we used the fertilized eggs from those F_0
524 adults to generate the F_1 generation by the second knockout, it could significantly
525 increase the simultaneous mutated probabilities of *bmp6a* and *bmp6b* because the
526 mutation of the F_1 progenies was the accumulation of the mutation inherited from the
527 F_0 germ cells and the mutation caused by the second knockout. This assumption was
528 evidenced by our results, in which the somatic mutation ratio in the F_1 generation was
529 significantly higher than that in the F_0 generation (Fig. 3(b-c); Supplementary Table
530 S5, S6). Thirdly, the mutants were screened using high-throughput sequencing
531 technology. Genome editing in cultured fishes needs to screen many individuals to
532 obtain as many mutants as possible, which is labor- and time-consumption by
533 traditional methods, such as gel electrophoresis, Sanger sequencing, high-resolution
534 melt curves, etc. Based on our previous study (Tong et al., 2018) , we developed a
535 mutant screening method using high-throughput sequencing of PCR products by
536 amplifying the target fragments using two pairs of primers, one of which was used to
537 amplify the fragment containing the gene editing target sites and the other pair was
538 used to append the index bases of the sample to the PCR product, after sequencing,
539 the data were demultiplexed to individuals and knockout targets which were used to
540 screen the mutants by CRISPResso2 (Fiume et al., 2019). Using this method, we can
541 obtain the mutants in a time- and cost-efficient way. This strategy has an advantage,
542 i.e., it could reduce the time to establish a new strain with both genes mutated from
543 3~4 generations to 2 generations; however, the disadvantage is that the strain has
544 multiple alleles (Supplementary Figs. S4-S10).
545 Using the strategy described above, we obtained the mutants without IMBs in the
546 F_1 population and established the WUCI strain in two generations; the observation of
547 IMB in the F_3 progenies suggested that the trait was stable and inheritable; these
548 results demonstrated that *bmp6* could be used to generate new cyprinids strains
549 without IMBs by gene editing.
550 *Bmp6* is a member of the BMP family, and it regulates many biological processes,
551 such as skeletal development (Wan and Cao, 2005), iron metabolism (Jr et al., 2009),
552 female fertility (Campbell et al., 2009; Sugiura et al., 2010), and so on. Although the
553 knockout of *bmp6* had no significant effects on growth and reproductive performance
554 or the development of muscle and skeletal in zebrafish (Jian et al., 2019; Xu et al.,
555 2022; Yang et al., 2021, 2020), it is unknown whether the knockout of *bmp6* affects
556 the performance of the WUCI strain. Here, we comprehensively evaluated growth,
557 reproduction, nutrient quality, muscle structure, and texture between the WUCI strain
558 and the wild-type crucian carp. The results showed that the knockout of *bmp6a* and
559 *bmp6b* did not affect the growth and reproductive performance of the WUCI strain,
560 which was consistent with our previous studies in zebrafish (Jian et al., 2019; Xu et
561 al., 2022; Yang et al., 2021, 2020) . Growth is associated with the development of
562 muscle and skeleton; the skeletal phenotype and the histological section of muscle
563 showed that the musculoskeletal development was normal in the WUCI strain,
564 implying that the function of *bmp6* in the musculoskeletal system might be
565 compensated by others of the BMP family (Solloway et al., 1998) . *Bmp6* is also
566 involved in proliferation, steroidogenesis, and oocyte development in humans and
567 mammals (Liu et al., 2019; Lochab and Extavour, 2017; Song et al., 2022; Sugiura et
568 al., 2010; Zhang et al., 2019) functions in a specifies-specific way(Regan et al., 2018).
569 Although the mRNA of *bmp6* was detected in oocytes and granulosa cells (Li and Ge,
570 2011) in zebrafish, there was no enough evidence to show the effect of *bmp6* on
571 female fecundity. The present study and our previous studies showed that the
572 knockout of *bmp6* did not significantly affect the reproductive performance in crucian

carp and zebrafish, which implied that *bmp6* might not be the essential gene in the gonadal development of cyprinids, or the function of *bmp6* is compensated by other members of the BMP/TGE-β family; however, more studies are required. The detection of 7 elements in the liver and muscle showed that the content of Fe was higher in the WUCI strain than that in the wild-type crucian carp, which indicated that the iron overload in the liver of the WUCI strain caused by the dysfunction of *bmp6* (Jr et al., 2009), however, the content of Fe in the muscle of the WUCI strain did not show the significance compared to that of the wild-type crucian carp, which meant the deposited and transferred mechanism of Fe in muscle might be different in the liver.

In addition to evaluating nutrient quality by the traditional method, we performed further analysis of the metabolome. Metabolomics analysis results showed some pathways and metabolites were enriched in the muscle tissue of the WUCI strain, such as Nicotinate and nicotinamide metabolism pathway, Thiamine metabolism pathway, β-Nicotinamide mononucleotide, DL-Glutamine, Hypoxanthine, and Betaine. These pathways and metabolites are related to beneficial properties, including anti-aging, anti-oxidative, and anti-radiation damage effects (Fig. 9). Nicotinate and nicotinamide are precursors of the coenzymes nicotinamide adenine dinucleotide (NAD+) and nicotinamide adenine dinucleotide phosphate (NADP+) that are essential for the generation of coenzymes (Information, 2022) . β-Nicotinamide mononucleotide is an important metabolite of the Nicotinate and nicotinamide metabolism pathway (Supplementary Fig. S13A). β-Nicotinamide mononucleotide is also a precursor of NAD+ and is considered a candidate compound for suppressing aging because it retained in the body for longer than Nicotinamide (KAWAMURA et al., 2016; Nadeeshani et al., 2021) . Thiamin is involved in several cell functions, including energy metabolism and the degradation of sugars and carbon skeletons (Manzetti et al., 2014). Thiamine pyrophosphate is the active form of thiamine and a member of the Thiamine metabolism pathway (Supplementary Fig. S13B) (Zeece, 2020) deficiencies can lead to various forms of beriberi (Nohr et al., 2011) . DL-Glutamine is the most abundant amino acid in the body. A recent study has shown that adding enteral L-glutamine to normal nutrition during the early stage of COVID-19 infection can shorten the hospital stay for patients (Cengiz et al., 2020) . Hypoxanthine is an intermediate metabolite in the purine degradation system and a substrate for ATP synthesis which can reduce the severity of radiation damage by increasing the survival of endothelial cells from DNA damage and apoptosis in mice (Fujiwara et al., 2022) . Betaine is lipotropic, an important human nutrient, and dietary betaine was utilized as an osmolyte and source of methyl groups, thereby helping maintain liver, heart, and kidney health(Craig, 2004).

5. Conclusion

Bmp6 is a key gene that regulates the development of intermuscular bones. For the two orthologs of *bmp6* in crucian carp genome, we established a two-round gene knockout and mating strategy to rapidly generate the new crucian carp strain without IMBs by knocking out *bmp6*. We cultured the WUCI strain to the F3 generation and characterized the strain outperformed the wild-type crucian carp in growth at 4-month age and did not show significant differences in the reproductive performance and flesh quality. The metabolomics analysis of the muscle tissues showed that the WUCI strain significantly enriched some metabolites plays beneficial effects in anti-aging, anti-oxidant, and anti-radiation damage. This study is the first report that a farmed cyprinid strain without IMBs, which could be stably inherited, was obtained in the world. This strain provides excellent germplasm for the cyprinids aquaculture industry.

Our gene editing strategy is a useful molecular tool for eliminating IMBs in other cyprinids and knocking out multiple orthologs rapidly.

Acknowledgments

We greatly thank Professor Ying Li at the Second Affiliated Hospital of Harbin Medical University for scanning mutants with X-ray and thank Dr. Yi Zhou at Harvard Medical School for providing technical support in CRISPR/Cas9. We also thank Professor Yumei Chang, Chitao Li, and Gefeng Xu at HRFRI for their support in the histological section and muscle texture analysis.

Funding

This study was supported by the National Key R&D Program of China (no. 2018YFD0900102), Central Public-interest Scientific Institution Basal Research Fund, CAFS (no. 2022YJ06, 2020XT0102), Central Public-interest Scientific Institution Basal Research Fund, HRFRI (no. HSY202108Q, HYS201802Z).

Declaration of Competing Interest

The authors declare no competing financial interests.

Ethics statement

In this study, all animal procedures were conducted according to the guidelines for the care and use of laboratory animals of Heilongjiang River Fisheries Research Institute (HRFRI), Chinese Academy of Fishery Sciences (CAFS). The studies in animals were reviewed and approved by the Committee for the Welfare and Ethics of Laboratory Animals of HRFRI, CAFS. The gene editing studies were approved by the Committee for Genetic Modification Organism (GMO) Safety Management (Approved ID: HRFRI-GMO-201801).

CRediT authorship contribution statement

Youyi Kuang: Conceptualization, Methodology, Writing-Original Draft ,Writing-Review & Editing, Supervision, Funding acquisition. **Xianhu Zheng**: Investigation, Resources. **Dingchen Cao:** Investigation, Resources. **Zhipeng Sun:** Investigation, Resources. **GuangxiangTong:** Investigation, Resources. **Huan Xu:** Writing-Original Draft ,Writing-Review & Editing, Formal analysis. **Ting Yan:** Investigation, Funding acquisition. **Shizhan Tang**: Investigation, Formal analysis. **Zhongxiang Chen:** Investigation, Formal analysis. **Tingting Zhang:** Investigation,Visualization. **Tan Zhang:** Investigation,Visualization. **Le Dong:** Investigation,Visualization. **Xiaoxing Yang:** Investigation,Visualization. **Huijie Zhou:** Investigation,Visualization. **Weilun Guo:** Investigation,Visualization. **Xiaowen Sun:** Conceptualization.

REFERENCES

Beliveau, B.J., Kishi, J.Y., Nir, G., Sasaki, H.M., Saka, S.K., Nguyen, S.C., Wu, C., Yin, P., 2018. OligoMiner provides a rapid, flexible environment for the design of genome-scale oligonucleotide in situ hybridization probes. Proc National Acad Sci 115, 201714530. https://doi.org/10.1073/pnas.1714530115

Campbell, B.K., Kendall, N.R., Baird, D.T., 2009. Effect of Direct Ovarian Infusion of Bone Morphogenetic Protein 6 (BMP6) on Ovarian Function in Sheep1. Biol Reprod 81, 1016–1023. https://doi.org/10.1095/biolreprod.109.076653

Cao, D.C., Kuang, Y.Y., Zheng, X. H., Tong, G.X., Li, C.T., Sun, X.W., 2015. Comparative analysis of intermuscular bones in three strains of common carp. J Appl Ichthyol 31, 32–36. https://doi.org/10.1111/jai.12483

Cengiz, M., Uysal, B.B., Ikitimur, H., Ozcan, E., Islamoğlu, M.S., Aktepe, E., Yavuzer, H., Yavuzer, S., 2020. Effect of oral l-Glutamine supplementation on Covid-19 treatment. Clin Nutrition Exp 33, 24–31. https://doi.org/10.1016/j.yclnex.2020.07.003

Chen, Z., Omori, Y., Koren, S., Shirokiya, T., Kuroda, T., Miyamoto, A., Wada, H., Fujiyama, A., Toyoda, A., Zhang, S., Wolfsberg, T.G., Kawakami, K., Phillippy, A.M., Program, N.C.S., Mullikin, J.C., Burgess, S.M., 2019. De novo assembly of the goldfish (Carassius auratus) genome and the evolution of genes after whole-genome duplication. Sci Adv 5, eaav0547. https://doi.org/10.1126/sciadv.aav0547

Craig, S.A., 2004. Betaine in human nutrition. Am J Clin Nutrition 80, 539–549. https://doi.org/10.1093/ajcn/80.3.539

Dharmaratnam, A., Sudhagar, A., Nithianantham, S.R., Das, S., Swaminathan, T.R., 2021. Evaluation of candidate reference genes for quantitative RTqPCR analysis in goldfish (Carassius auratus L.) in healthy and CyHV-2 infected fish. Vet Immunol Immunop 237, 110270. https://doi.org/10.1016/j.vetimm.2021.110270

Fiume, M., Cupak, M., Keenan, S., Rambla, J., Torre, S. de la, Dyke, S.O.M., Brookes, A.J., Carey, K., Lloyd, D., Goodhand, P., Haeussler, M., Baudis, M., Stockinger, H., Dolman, L., Lappalainen, I., Törnroos, J., Linden, M., Spalding, J.D., Ur Rehman, S., Page, A., Flicek, P., Sherry, S., Haussler, D., Varma, S., Saunders, G., Scollen, S., 2019. CRISPResso2 provides accurate and rapid genome editing sequence analysis. Nat Biotechnol 37, 224–226. https://doi.org/10.1038/s41587-019-0032-3

Franěk, R., Kašpar, V., Shah, M.A., Gela, D., Pšenička, M., 2021. Production of common carp donor-derived offspring from goldfish surrogate broodstock. Aquaculture 534, 736252. https://doi.org/10.1016/j.aquaculture.2020.736252

Fujiwara, M., Sato, N., Okamoto, K., 2022. Hypoxanthine Reduces Radiation Damage in Vascular Endothelial Cells and Mouse Skin by Enhancing ATP Production via the Salvage Pathway. Radiat Res 197, 583–593. https://doi.org/10.1667/rade-21-00223.1

Gan, R.H., Wang, Y., Li, Z., Yu, Z.X., Li, X.Y., Tong, J.F., Wang, Z.W., Zhang, X.J., Zhou, L., Gui, J.F., 2021. Functional Divergence of Multiple Duplicated Foxl2 Homeologs and Alleles in a Recurrent Polyploid Fish. Mol Biol Evol 38, 1995–2013. https://doi.org/10.1093/molbev/msab002

Gjedrem, T., 1997. Flesh quality improvement in fish through breeding. Aquaculture international 5, 197 206.

Gui, J.F., Zhou, L., Li, X.Y., 2021. Rethinking fish biology and biotechnologies in the challenge era for burgeoning genome resources and strengthening food security. Water Biology Secur 100002. https://doi.org/10.1016/j.watbs.2021.11.001

Information, N., Center for Biotechnology, 2022. PubChem Pathway Summary for Pathway SMP0087241, Nicotinate and Nicotinamide Metabolism, Source: PathBank. Retrieved November 15, 2022 from https://pubchem.ncbi.nlm.nih.gov/pathway/PathBank:SMP0087241.

Jian, Y., Guangxiang, T., Xianhu, Z., Zhipeng, S., Weihua, L., Xiaowen, S., Youyi, K., 2019. Comparative analysis of embryonic muscle development in wildtype zebrafish and its intermuscular bone deficiency mutant. Journal of Fishery Sciences of China 26, 296–303.

Jr, B., Andriopoulos, Corradini, E., Xia, Y., Faasse, S.A., Chen, S., Grgurevic, L., Knutson, M.D., Pietrangelo, A., Vukicevic, S., Lin, H.Y., Babitt, J.L., 2009. BMP6 is a key endogenous regulator of hepcidin expression and iron metabolism. Nat Genet 41, 482–487. https://doi.org/10.1038/ng.335

Kague, E., Hughes, S.M., Lawrence, E.A., Cross, S., Martin Silverstone, E., Hammond, C.L., Hinits, Y., 2019. Scleraxis genes are required for normal musculoskeletal development and for rib growth and mineralization in zebrafish. Faseb J 33, 9116–9130. https://doi.org/10.1096/fj.201802654rr

KAWAMURA, T., MORI, N., SHIBATA, K., 2016. β-Nicotinamide Mononucleotide, an Anti-Aging Candidate Compound, Is Retained in the Body for Longer than Nicotinamide in Rats. J Nutr Sci Vitaminol 62, 272–276. https://doi.org/10.3177/jnsv.62.272

740 Kishi, J.Y., Lapan, S.W., Beliveau, B.J., West, E.R., Zhu, A., Sasaki, H.M., Saka,
741 S.K., Wang, Y., Cepko, C.L., Yin, P., 2019. SABER amplifies FISH: enhanced
742 multiplexed imaging of RNA and DNA in cells and tissues. Nat Methods 16,
743 533–544. https://doi.org/10.1038/s41592-019-0404-0

744 Kishi, J.Y., Schaus, T.E., Gopalkrishnan, N., Xuan, F., Yin, P., 2018. Programmable
745 autonomous synthesis of single-stranded DNA. Nat Chem 10, 155–164.
746 https://doi.org/10.1038/nchem.2872

747 Labun, K., Montague, T.G., Krause, M., Torres Cleuren, Y.N., Tjeldnes, H., Valen, E.,
748 2019. CHOPCHOP v3: expanding the CRISPR web toolbox beyond genome
749 editing. Nucleic Acids Res 47, W171–W174. https://doi.org/10.1093/nar/gkz365

750 Li, C.W., Ge, W., 2011. Spatiotemporal Expression of Bone Morphogenetic Protein
751 Family Ligands and Receptors in the Zebrafish Ovary: A Potential
752 Paracrine-Signaling Mechanism for Oocyte-Follicle Cell Communication. Biol
753 Reprod 85, 977–986. https://doi.org/10.1095/biolreprod.111.092239

754 Li, L., Zhong, Z., Zeng, M., Liu, S., Zhou, Y., Xiao, J., Wang, J., Liu, Y., 2013.
755 Comparative analysis of intermuscular bones in fish of different ploidies. Sci
756 China Life Sci 56, 341–350. https://doi.org/10.1007/s11427-013-4465-5

757 Liu, Y., Chen, M., Zhao, X., Ren, X., Shao, S., Zou, M., Zhang, L., 2019. Bone
758 morphogenetic protein 6 expression in cumulus cells is negatively associated with
759 oocyte maturation. Hum Fertil 24, 290–297.
760 https://doi.org/10.1080/14647273.2019.1660003

761 Lochab, A.K., Extavour, C.G., 2017. Bone Morphogenetic Protein (BMP) signaling in
762 animal reproductive system development and function. Dev Biol 427, 258–269.
763 https://doi.org/10.1016/j.ydbio.2017.03.002

764 Manzetti, S., Zhang, J., Spoel, D. van der, 2014. Thiamin Function, Metabolism,
765 Uptake, and Transport. Biochemistry 53, 821–835.
766 https://doi.org/10.1021/bi401618y

767 Meske, C., 1968. Breeding carp for reduced number of intermuscular bones, and
768 growth of carp in aquaria. Bamidgeh, Bulletin of Fish Culture in Israel 20,
769 105–119.

770 Nadeeshani, H., Li, J., Ying, T., Zhang, B., Lu, J., 2021. Nicotinamide
771 Mononucleotide (NMN) as an Anti-Aging Health Product - Promises and Safety
772 Concerns. J Adv Res 37, 267–278. https://doi.org/10.1016/j.jare.2021.08.003

773 Nie, C., Hilsdorf, A.W.S., Wan, S., Gao, Z., 2020. Understanding the development of
774 intermuscular bones in teleost: status and future directions for aquaculture. Rev
775 Aquacult 12, 759–772. https://doi.org/10.1111/raq.12348

776 Nie, C., Wan, S., Chen, Y., Zhu, D., Wang, X., Dong, X., Gao, Z.X., 2021. Loss of
777 scleraxis leads to distinct reduction of mineralized intermuscular bone in zebrafish.
778 Aquac Fish 6, 169–177. https://doi.org/10.1016/j.aaf.2020.04.006

779 Nohr, D., Biesalski, H.K., Back, E.I., 2011. Encyclopedia of Dairy Sciences (Second
780 Edition). Article Titles V 701–703.
781 https://doi.org/10.1016/b978-0-12-374407-4.00490-8

782 Pang, Z., Zhou, G., Ewald, J., Chang, L., Hacariz, O., Basu, N., Xia, J., 2022. Using
783 MetaboAnalyst 5.0 for LC–HRMS spectra processing, multi-omics integration and
784 covariate adjustment of global metabolomics data. Nat Protoc 17, 1735–1761.
785 https://doi.org/10.1038/s41596-022-00710-w

786 Perazza, C.A., Menezes, J.T.B. de, Ferraz, J.B.S., Pinaffi, F.L.V., Silva, L.A.,
787 Hilsdorf, A.W.S., 2017. Lack of intermuscular bones in specimens of Colossoma
788 macropomum: An unusual phenotype to be incorporated into genetic improvement
789 programs. Aquaculture 472, 57 60.
790 https://doi.org/10.1016/j.aquaculture.2016.05.014

791 Regan, S.L.P., Knight, P.G., Yovich, J.L., Leung, Y., Arfuso, F., Dharmarajan, A.,
792 2018. Chapter Nine Involvement of Bone Morphogenetic Proteins (BMP) in the
793 Regulation of Ovarian Function. Vitam Horm 107, 227–261.
794 https://doi.org/10.1016/bs.vh.2018.01.015

795 Solloway, M.J., Dudley, A.T., Bikoff, E.K., Lyons, K.M., Hogan, B.L.M., Robertson,
796 E.J., 1998. Mice lacking Bmp6 function. Dev Genet 22, 321–339.
797 https://doi.org/10.1002/(sici)1520-6408(1998)22:4<321::aid-dvg3>3.0.co;2-8

798 Song, S., Ding, W., Yao, H., Wang, L., Li, B., Wang, Y., Tang, X., Zhang, Y., Huang,
799 D., Xu, D., Zhao, Z., 2022. BMP6 Promotes the Secretion of 17 Beta-Estradiol and
800 Progesterone in Goat Ovarian Granulosa Cells. Animals Open Access J Mdpi 12,
801 2132. https://doi.org/10.3390/ani12162132

802 Sugiura, K., Su, Y.Q., Eppig, J.J., 2010. Does Bone Morphogenetic Protein 6 (BMP6)
803 Affect Female Fertility in the Mouse?1. Biol Reprod 83, 997–1004.
804 https://doi.org/10.1095/biolreprod.110.086777

805 Sun, Y., Zhu, Z., 2019. Designing future farmed fishes using genome editing. Sci
806 China Life Sci 62, 420–422. https://doi.org/10.1007/s11427-018-9467-x

807 Tang, G., Lv, W., Sun, Z., Cao, D., Zheng, X., Tong, G., Wang, H., Zhang, X., Kuang,
808 Y., 2020. Heritability and quantitative trait locus analyses of intermuscular bones
809 in mirror carp (Cyprinus carpio). Aquaculture 515, 734601.
810 https://doi.org/10.1016/j.aquaculture.2019.734601

811 Tong, G., Xu, W., Zhang, Y., Zhang, Q., Yin, J., Kuang, Y., 2018. De novo assembly
812 and characterization of the Hucho taimen transcriptome. Ecol Evol 8, 1271 1285.
813 https://doi.org/10.1002/ece3.3735

814 Wan, M., Cao, X., 2005. BMP signaling in skeletal development. Biochem Bioph Res
815 Co 328, 651–657. https://doi.org/10.1016/j.bbrc.2004.11.067

816 Wan, S.M., Xiong, X.M., Tomljanović, T., Chen, Y.L., Liu, H., Treer, T., Gao, Z.X.,
817 2019. Identification and mapping of SNPs associated with number of
818 intermuscular bone in blunt snout bream. Aquaculture 507, 75–82.
819 https://doi.org/10.1016/j.aquaculture.2019.04.013

820 Wu, C., Huang, X., Chen, Q., Hu, F., Zhou, L., Gong, K., Fu, W., Gong, D., Zhao, R.,
821 Zhang, C., Qin, Q., Tao, M., Liu, S., 2020. The formation of a new type of hybrid
822 culter derived from a hybrid lineage of Megalobrama amblycephala (♀) × Culter
823 alburnus (♂). Aquaculture 525, 735328.
824 https://doi.org/10.1016/j.aquaculture.2020.735328

825 Wu, R.S., Lam, I.I., Clay, H., Duong, D.N., Deo, R.C., Coughlin, S.R., 2018. A Rapid
826 Method for Directed Gene Knockout for Screening in G0 Zebrafish. Dev Cell 46,
827 112-125.e4. https://doi.org/10.1016/j.devcel.2018.06.003

828 Xiong, X.M., Robinson, N.A., Zhou, J.J., Chen, Y.L., Wang, W., Wang, X.B., Gao,
829 Z.X., 2019. Genetic parameter estimates for intermuscular bone in blunt snout
830 bream (Megalobrama amblycephala) based on a microsatellite-based pedigree.
831 Aquaculture 502, 371–377. https://doi.org/10.1016/j.aquaculture.2018.12.072

832 Xu, H., Tong, G., Yan, T., Dong, L., Yang, X., Dou, D., Sun, Z., Liu, T., Zheng, X.,
833 Yang, J., Sun, X., Zhou, Y., Kuang, Y., 2022. Transcriptomic Analysis Provides
834 Insights to Reveal the bmp6 Function Related to the Development of Intermuscular
835 Bones in Zebrafish. Frontiers Cell Dev Biology 10, 821471.
836 https://doi.org/10.3389/fcell.2022.821471

837 XU, X., ZHENG, J., QIAN, Y., LUO, C., 2015. Normally grown and developed
838 intermuscular bone-deficient mutant in grass carp, Ctenopharyngodon idellus.
839 Chinese Sci Bull 60, 52–57. https://doi.org/10.1360/n972014-00637

840 Yang, J., Tong, G., Sun, Z., Zheng, X., Lv, W., Cao, D., Sun, X., Kuang, Y., 2021.
841 Comparative Analysis of Muscle Development in Zebrafish with Different

842 Intermuscular Bones Patterns. Pak J Zool 53, 313–322.
843 https://doi.org/10.17582/journal.pjz/20181125111102

844 Yang, J., Tong, G., Zheng, X., Sun, Z., Lv, W., Sun, X., Kuang, Y., 2020.
845 Comparative analysis of skeletal development between wildtype zebrafish and
846 intermuscular bone-deficient mutants. Acta Hydrobiologica Sinica 44, 546–553.

847 Zeece, M., 2020. Introduction to the Chemistry of Food 163–212.
848 https://doi.org/10.1016/b978-0-12-809434-1.00005-0

849 Zhang, X.Y., Chang, H.M., Zhu, H., Liu, R.Z., Leung, P.C.K., 2019. BMP6 increases
850 TGF-β1 production by up-regulating furin expression in human granulosa-lutein
851 cells. Cell Signal 55, 109–118. https://doi.org/10.1016/j.cellsig.2019.01.002

852
853
854 **Figure legends**
855
856 **Fig. 1. Expression of *bmp6a* and *bmp6b* in tissues of crucian carp.** (a): the gene
857 tree of *bmp6a* and *bmp6b*, the tree was extracted from Ensembl. (b): the expression of
858 *bmp6a* and *bmp6b* in crucian carp tissues analyzed by qPCR, electrophoretic images
859 were cropped from the original images in Supplementary Figs. S1, S2. M: molecular
860 marker. (c): the relative expression levels of *bmp6a* and *bmp6b* in crucian carp tissues
861 analyzed by real-time quantitative PCR. (d) and (e): spatial expression of *bmp6a* (d)
862 and *bmp6b* (e) in caudal muscle, the white dashed lines indicate myospetum; mRNA
863 of *bmp6a*(d) *and bmp6b*(e) were detected with Alexa Fluro 532 labeled probes (left),
864 the nucleus was stained with DAPI dye (middle), and the merged images were shown
865 in the right; scale bar: 100μm.
866
867 **Fig. 2. Pipeline for generating the new crucian carp strain without intermuscular**
868 **bones.** (a): the schematic diagram for constructing the new strain without
869 intermuscular bones. (b): target sites of *bmp6a* and *bmp6b* for CRISPR/Cas9
870 knockout. (c): the schematic diagram for screening mutants.
871
872 **Fig. 3. Observation of intermuscular bones in mutants of F_1, F_2, and F_3**
873 **generations.** (a): timeline of this study. (b): the somatic mutation distribution of
874 mutants in the F_0 and F_1 generation. (c): the somatic mutation distribution of mutants
875 with both genes mutated in the F_0 and F_1 generation. (d): in-frame mutation
876 distribution of mutants in the F_0 and F_1 generation. (e): frame-shift mutation
877 distribution of mutants in the F_0 and F_1 generation. (f): micro-CT images of a
878 wild-type crucian carp (top) and a representative mutant without intermuscular bones
879 in the F_1 generation(bottom). (g): X-ray images of a wild-type crucian carp (top left)
880 and representative mutants of single gene knockout homozygous line of *bmp6a*$^{-/-}$ (top
881 right), *bmp6b*$^{-/-}$ mutant (bottom left), and *bmp6a*$^{-/-}$/*bmp6b*$^{-/-}$ (bottom right) in the F_2
882 generation. (h): X-ray images of a wild-type crucian carp(top) and a representative
883 mutant without intermuscular bones(bottom) in the F_3 generation. (i): skeletal staining
884 images of a wild-type crucian carp(top) and a representative mutant without
885 intermuscular bones(bottom) in the F_3 generation, 41 individuals were randomly
886 chosen for bone staining, and no intermuscular bones were observed; top left, caudal

skeleton; top right, dorsal skeleton. The scale bar in (g) and (h) was 10mm, and the scale bar in (i) was 2000μm.

Fig. 4. Growth performance of the new strain without intermuscular bones and the wild-type crucian carp. The body length (SL, a) and body weight (BW, b) were measured at the age of 2, 3, and 4 months, the increment of SL(d) and BW(e) per month and the specific growth rate per month of SL(c) and BW(f) was calculated. The summary of BW and SL were listed in Supplementary Table S7. The significant difference was tested using Student's t-test. WT: the wild-type crucian carp; WUCI: the new strain without intermuscular bones; *: $P<0.05$; **: $P<0.01$; ***: $P<0.001$; ****: $P<0.0001$; ns: no significance.

Fig. 5. Nutrient quality of the new strain without intermuscular bones and the wild-type crucian carp. Proximate composition(a), total saccharide(b), vitamins(c), amino acid composition(d), and fatty acid (e, f) were determined. The data used to draw these figures were shown in Supplementary Table S8-S11. Wilcoxon test was used to test the significant levels (n=3). WT: the wild-type crucian carp; WUCI: the new strain without intermuscular bones; Ash: crude ash; Fat: crude fat; Protein: crude protein; Saccharide: total saccharide; VB1: vitamin B1; VB2: vitamin B2; VE: vitamin E; EAA: essential amino acid; TAA: total amino acid; UAA: umami amino acid; EFA: essential fatty acid; Saturated: saturated fatty acid; TFA: total fatty acid; Unsaturated: unsaturated fatty acid; MUFA: monounsaturated fatty acid; PUFA: polyunsaturated fatty acid; Omega3: omega3 fatty acid; Omega6: omega6 fatty acid; ns: no significance.

Fig. 6. Content of 7 elements in the new strain without intermuscular bones and the wild-type crucian carp. The contents of Mg(a), Mn(b), Fe(c), Cu(d), Zn(e), Se(f), and K(g) in the new strain, and the wild-type crucian carp were determined using the dorsal muscle and liver tissues. The data used to draw these figures were listed in Supplementary Table S12. Wilcoxon test was used to test the significant levels(n=5). WT: the wild-type crucian carp; WUCI: the new strain without intermuscular bones; *: $P<0.05$; ns: no significance.

Fig. 7. Muscle texture and structure of the new strain without intermuscular bones and the wild-type crucian carp. The shear force(a), hardness(b), cohesiveness(c), springiness(d), gumminess(e), and chewiness(f) were tested using a texture meter; Student's t-test was used to test the significant levels(n=30). The histological sections were carried out using dorsal muscle in the wild-type crucian carp(i) and the new strain(j), and the area(g) and density(h) of muscle fibers were calculated using the histological images with the ImageJ program, Wilcoxon test(n=5) was used to test the significant levels. The data used to draw the figures were shown in Supplementary Table S13. The scale bar in (i) and (j) was 50μm. WT: the wild-type crucian carp; WUCI: the new strain without intermuscular bones; *: $P<0.05$; **: $P<0.01$; ns: no significance.

Fig. 8. Reproductive performance of the new strain and the wild-type crucian carp. The weight of gonad(a), gonad index (GSI, b), female absolute fecundity(c), and relative fecundity(d) were compared between the 4-months-old individuals of the new strain and the wild-type crucian carp. The data used to draw the figures were shown in Supplementary Table S14; the Wilcoxon test was used to test the significant

levels. (e), histological sections of gonads in the wild-type crucian carp and the new strain, the scale bar in ovary and testis tissues was 100μm and 20μm, respectively. WT: the wild-type crucian carp; WUCI: the new strain without intermuscular bones; I(black arrowhead), II, III, and IV represent the developmental phases of oocytes; sg: Spermatogonium; sc: spermatocytes; SZ: Spermatozoa; *: $P<0.05$; ns: no significance.

Fig. 9. Metabolomics analysis of the new strain and the wild-type crucian carp. The PCA analysis of the metabolites in positive ion mode(a) and negative ion mode(b); The PLS-DA analysis of the metabolites in positive ion mode(c) and negative ion mode(d); (e-l): up-regulated metabolites in the WUCI strain. (m): the enriched pathways of metabolites in muscle tissue of the new strain analyzed by MetaboAnalyst 5.0. WT_M: muscle of wild-type crucian; WUCI_M: muscle of the new strain without intermuscular bones. ***：$P<0.001$

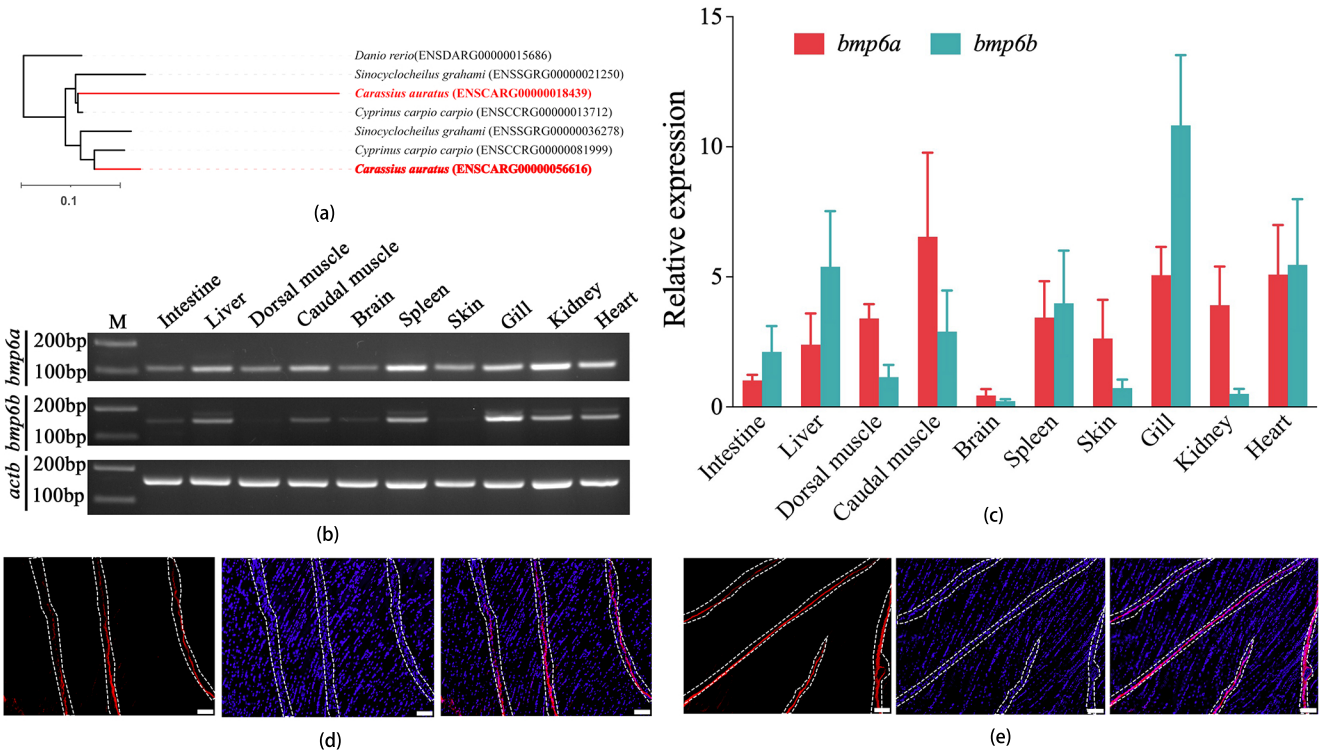
Danio rerio(ENSDARG00000015686)
Sinocyclocheilus grahami (ENSSGRG00000021250)
Carassius auratus (ENSCARG00000018439)
Cyprinus carpio carpio (ENSCCRG00000013712)
Sinocyclocheilus grahami (ENSSGRG00000036278)
Cyprinus carpio carpio (ENSCCRG00000081999)
Carassius auratus (ENSCARG00000056616)
0.1
(a)
M
Intestine
Liver
Dorsal muscle
Caudal muscle
Brain
Spleen
Skin
Gill
Kidney
Heart
bmp6a
bmp6b
actb
200bp
100bp
(b)
bmp6a
bmp6b
Relative expression
15
10
5
0
(c)
(d)
(e)

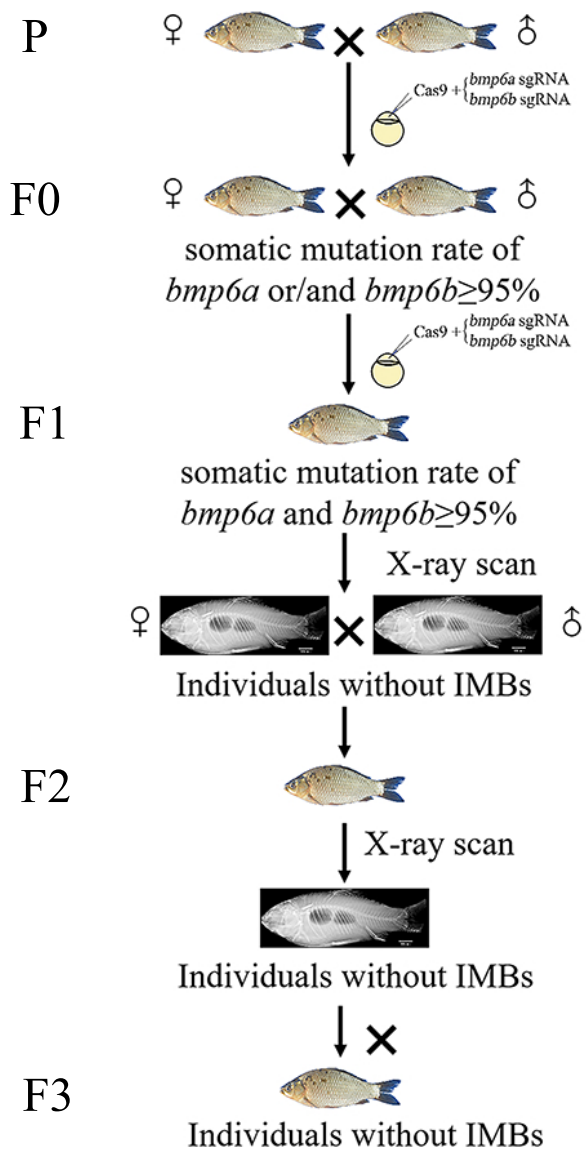
P
Cas9 + bmp6a sgRNA bmp6b sgRNA
F0
somatic mutation rate of bmp6a or/and bmp6b≥95%
Cas9 + bmp6a sgRNA bmp6b sgRNA
F1
somatic mutation rate of bmp6a and bmp6b≥95%
X-ray scan
Individuals without IMBs
F2
X-ray scan
Individuals without IMBs
F3
Individuals without IMBs

(a)

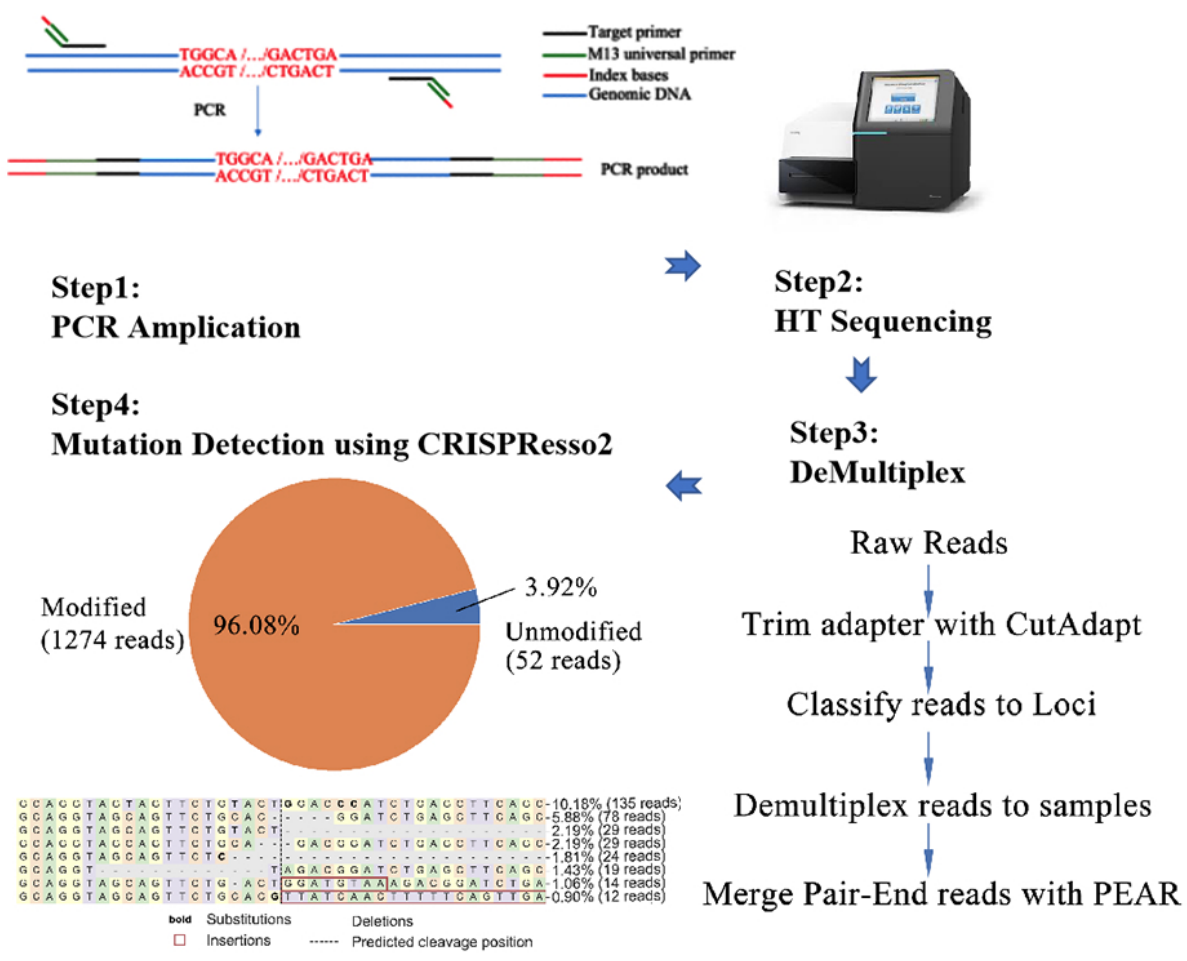
Target primer
M13 universal primer
Index bases
Genomic DNA
PCR
PCR product
Step1:
PCR Amplication
Step2:
HT Sequencing
Step3:
DeMultiplex
Step4:
Mutation Detection using CRISPResso2
Modified
(1274 reads)
96.08%
3.92%
Unmodified
(52 reads)
Raw Reads
Trim adapter with CutAdapt
Classify reads to Loci
Demultiplex reads to samples
Merge Pair-End reads with PEAR
Substitutions
Deletions
Insertions
Predicted cleavage position

(c)

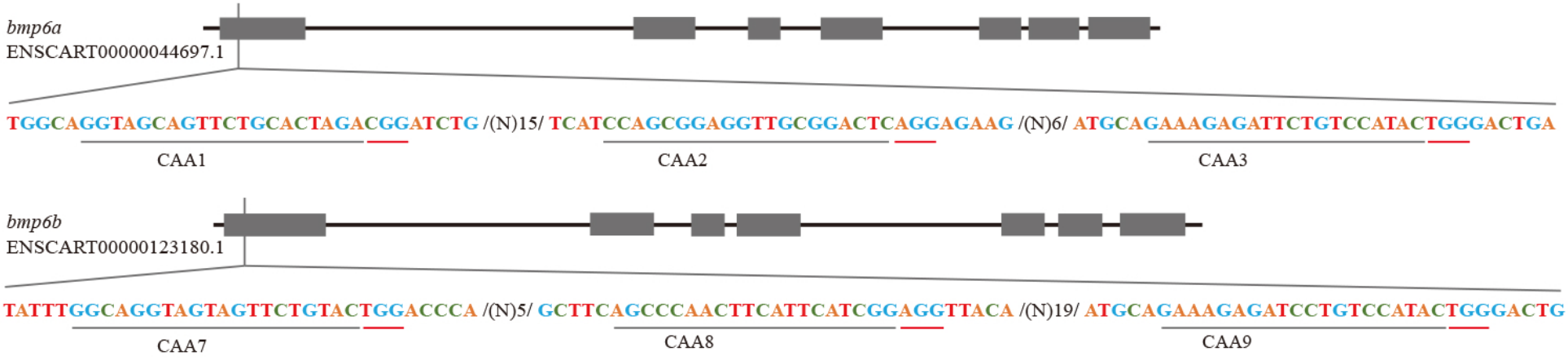
bmp6a
ENSCART00000044697.1
TGGCAGGTAGCAGTTCTGCACTAGACGGATCTG /(N)15/ TCATCCAGCGGAGGTTGCGGACTCAGGAGAAG /(N)6/ ATGCAGAAAGAGATTCTGTCCATACTGGGACTGA
CAA1
CAA2
CAA3
bmp6b
ENSCART00000123180.1
TATTTGGCAGGTAGTAGTTCTGTACTGGACCCA /(N)5/ GCTTCAGCCCAACTTCATTCATCGGAGGTTACA /(N)19/ ATGCAGAAAGAGATCCTGTCCATACTGGGACTG
CAA7
CAA8
CAA9

(b)

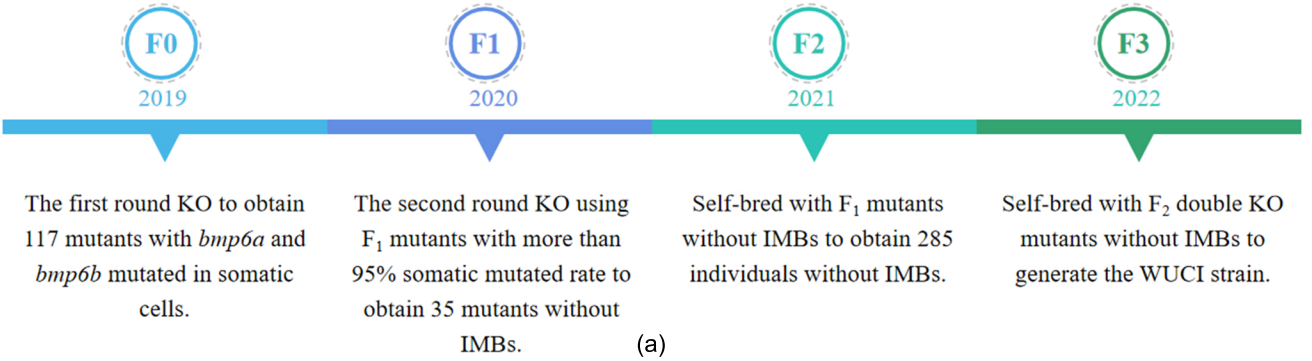
F0
2019
F1
2020
F2
2021
F3
2022
The first round KO to obtain 117 mutants with *bmp6a* and *bmp6b* mutated in somatic cells.
The second round KO using F_1 mutants with more than 95% somatic mutated rate to obtain 35 mutants without IMBs.
Self-bred with F_1 mutants without IMBs to obtain 285 individuals without IMBs.
Self-bred with F_2 double KO mutants without IMBs to generate the WUCI strain.

(a)

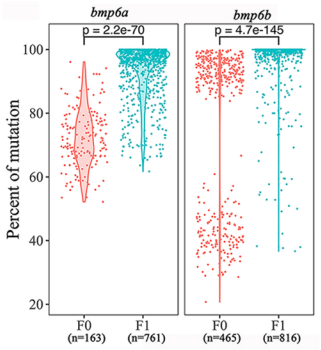
bmp6a
bmp6b
p = 2.2e-70
p = 4.7e-145
Percent of mutation
F0 (n=163)
F1 (n=761)
F0 (n=465)
F1 (n=816)

(b)

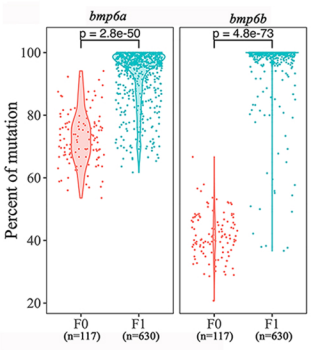
bmp6a
bmp6b
p = 2.8e-50
p = 4.8e-73
Percent of mutation
F0 (n=117)
F1 (n=630)
F0 (n=117)
F1 (n=630)

(c)

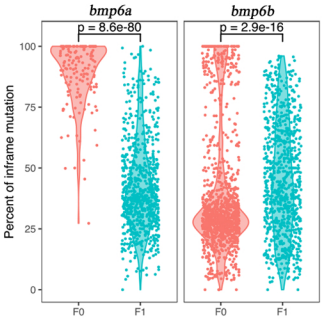
bmp6a
bmp6b
p = 8.6e-80
p = 2.9e-16
Percent of inframe mutation
F0
F1
F0
F1

(d)

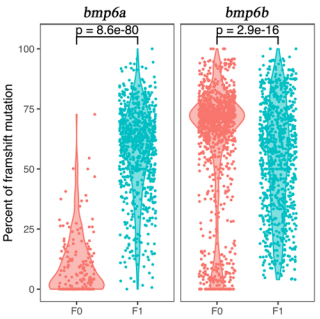
bmp6a
bmp6b
p = 8.6e-80
p = 2.9e-16
Percent of framshift mutation
F0
F1
F0
F1

(e)

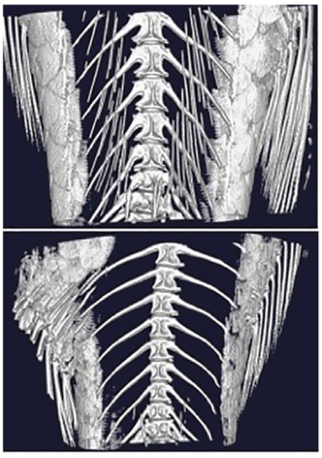

(f)

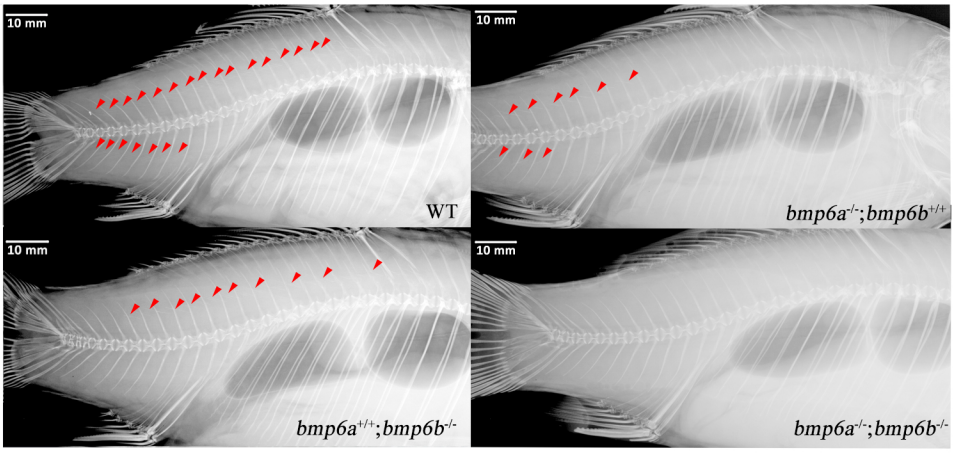
10 mm
WT
10 mm
bmp6a-/-;bmp6b+/+
10 mm
bmp6a+/+;bmp6b-/-
10 mm
bmp6a-/-;bmp6b-/-

(g)

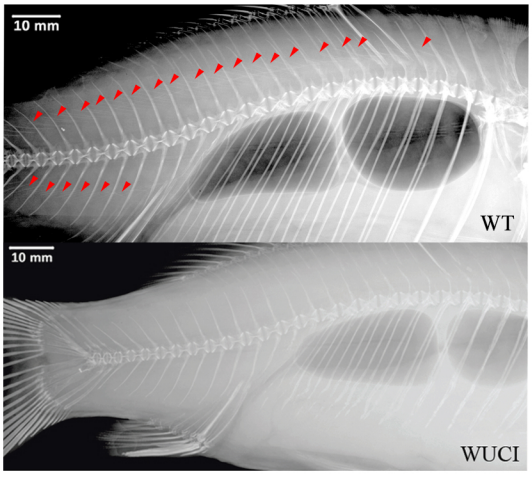
10 mm
WT
10 mm
WUCI

(h)

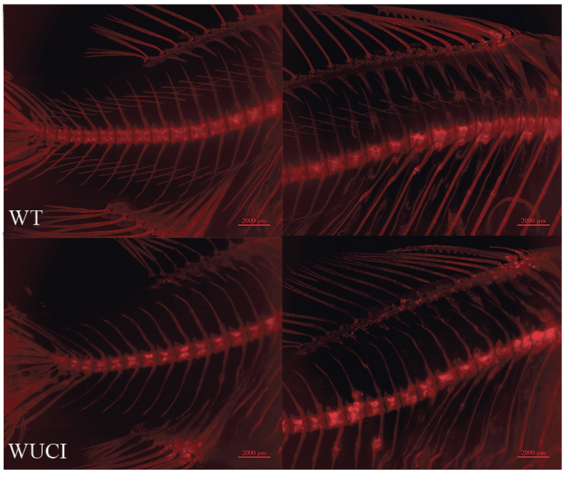
WT
WUCI

(i)

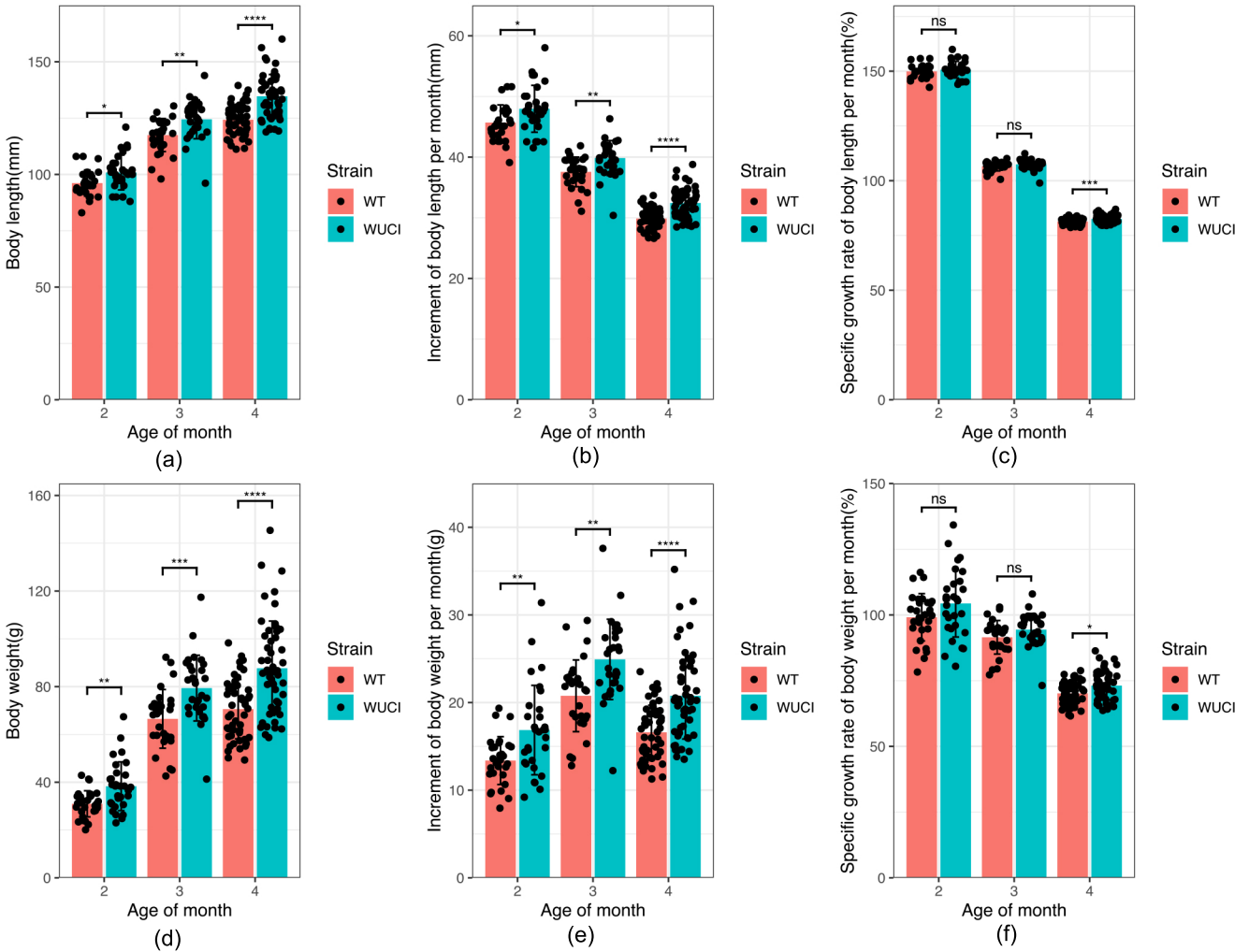
Body length(mm)
Age of month
Strain
WT
WUCI
(a)
Increment of body length per month(mm)
(b)
Specific growth rate of body length per month(%)
(c)
Body weight(g)
(d)
Increment of body weight per month(g)
(e)
Specific growth rate of body weight per month(%)
(f)

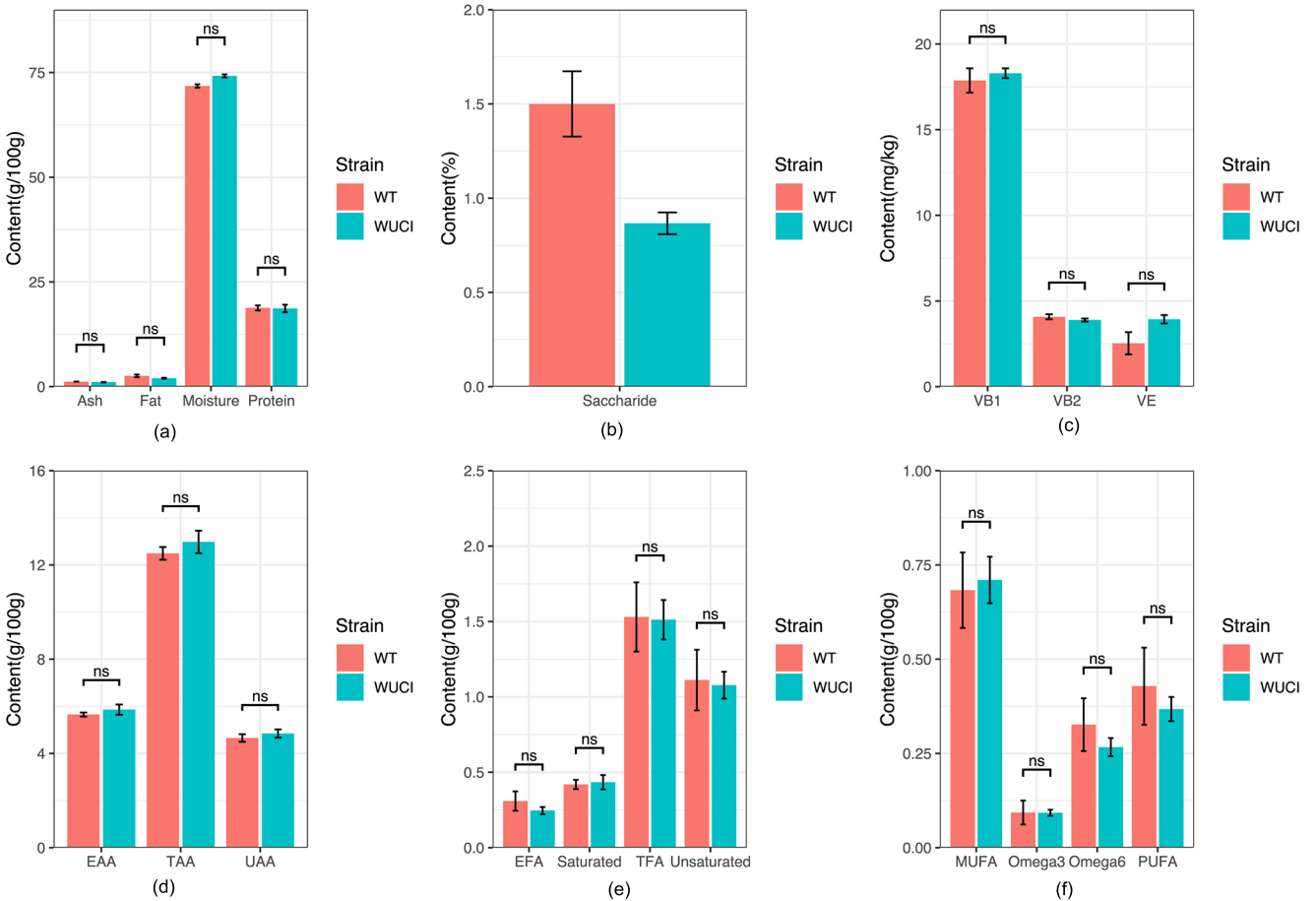
Content(g/100g)
ns
Ash
Fat
Moisture
Protein
(a)
Content(%)
Saccharide
(b)
Content(mg/kg)
VB1
VB2
VE
(c)
EAA
TAA
UAA
(d)
EFA
Saturated
TFA
Unsaturated
(e)
MUFA
Omega3
Omega6
PUFA
(f)
Strain
WT
WUCI

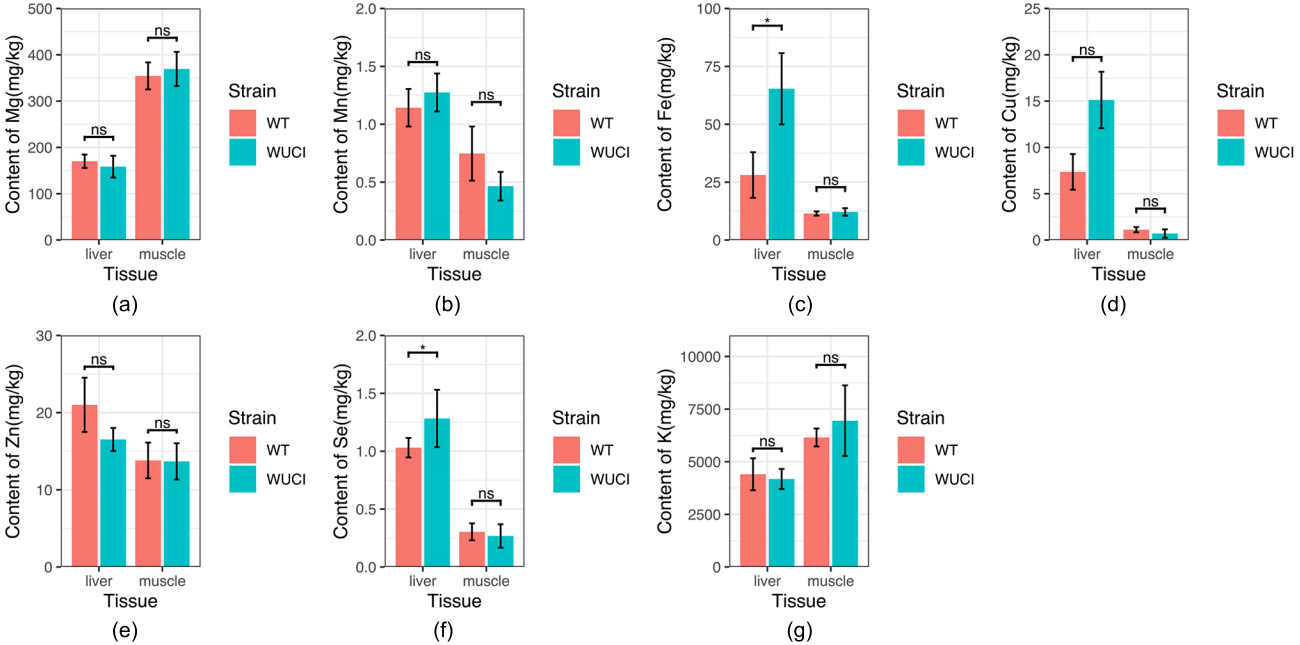
Content of Mg(mg/kg)
500
400
300
200
100
0
ns
ns
liver
muscle
Tissue
Strain
WT
WUCI
(a)
Content of Mn(mg/kg)
2.0
1.5
1.0
0.5
0.0
ns
ns
liver
muscle
Tissue
Strain
WT
WUCI
(b)
Content of Fe(mg/kg)
100
75
50
25
0
*
ns
liver
muscle
Tissue
Strain
WT
WUCI
(c)
Content of Cu(mg/kg)
25
20
15
10
5
0
ns
ns
liver
muscle
Tissue
Strain
WT
WUCI
(d)
Content of Zn(mg/kg)
30
20
10
0
ns
ns
liver
muscle
Tissue
Strain
WT
WUCI
(e)
Content of Se(mg/kg)
2.0
1.5
1.0
0.5
0.0
*
ns
liver
muscle
Tissue
Strain
WT
WUCI
(f)
Content of K(mg/kg)
10000
7500
5000
2500
0
ns
ns
liver
muscle
Tissue
Strain
WT
WUCI
(g)

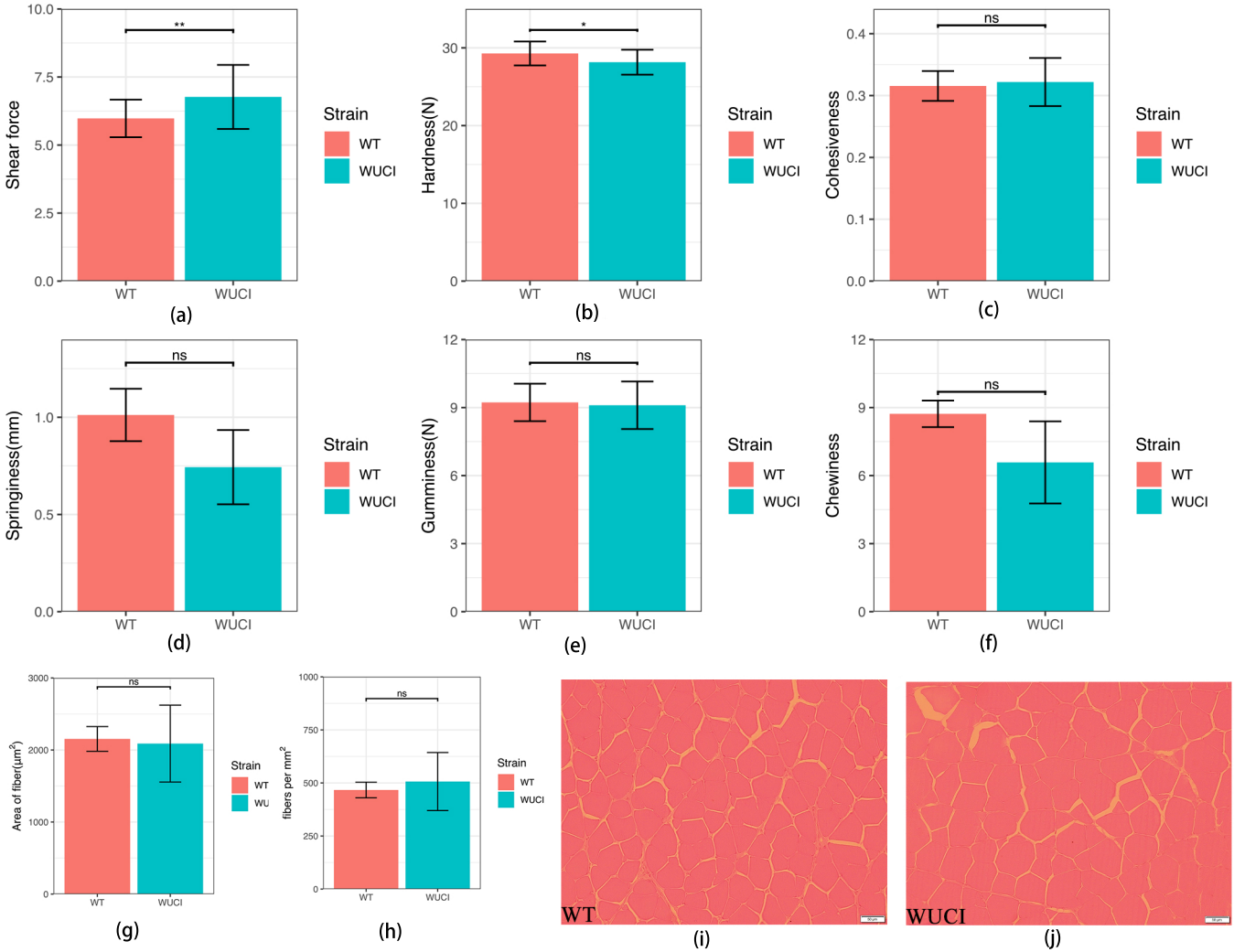
Shear force
10.0
7.5
5.0
2.5
0.0
**
WT
WUCI
(a)
Strain
WT
WUCI
Hardness(N)
30
20
10
0
*
WT
WUCI
(b)
Strain
WT
WUCI
Cohesiveness
0.4
0.3
0.2
0.1
0.0
ns
WT
WUCI
(c)
Strain
WT
WUCI
Springiness(mm)
1.0
0.5
0.0
ns
WT
WUCI
(d)
Strain
WT
WUCI
Gumminess(N)
12
9
6
3
0
ns
WT
WUCI
(e)
Strain
WT
WUCI
Chewiness
12
9
6
3
0
ns
WT
WUCI
(f)
Strain
WT
WUCI
Area of fiber(μm²)
3000
2000
1000
0
ns
WT
WUCI
(g)
Strain
WT
WU
fibers per mm²
1000
750
500
250
0
ns
WT
WUCI
(h)
Strain
WT
WUCI
WT
(i)
WUCI
(j)

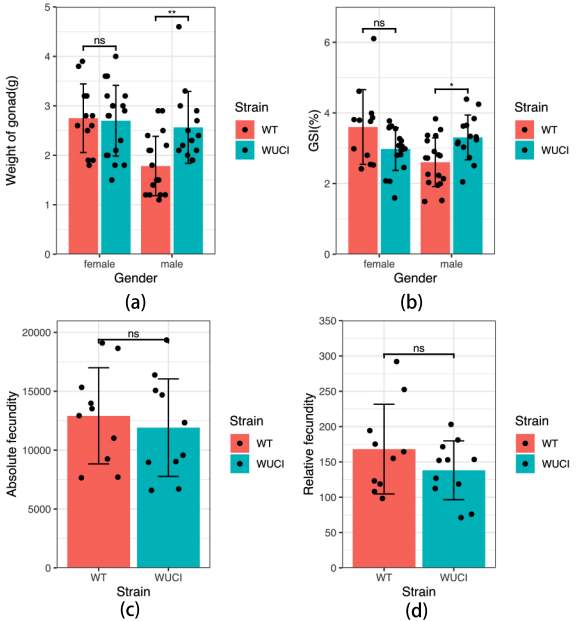
Weight of gonad(g)
ns
**
female
male
Gender
Strain
WT
WUCI
(a)
GSI(%)
ns
*
female
male
Gender
Strain
WT
WUCI
(b)
Absolute fecundity
ns
WT
WUCI
Strain
Strain
WT
WUCI
(c)
Relative fecundity
ns
WT
WUCI
Strain
Strain
WT
WUCI
(d)

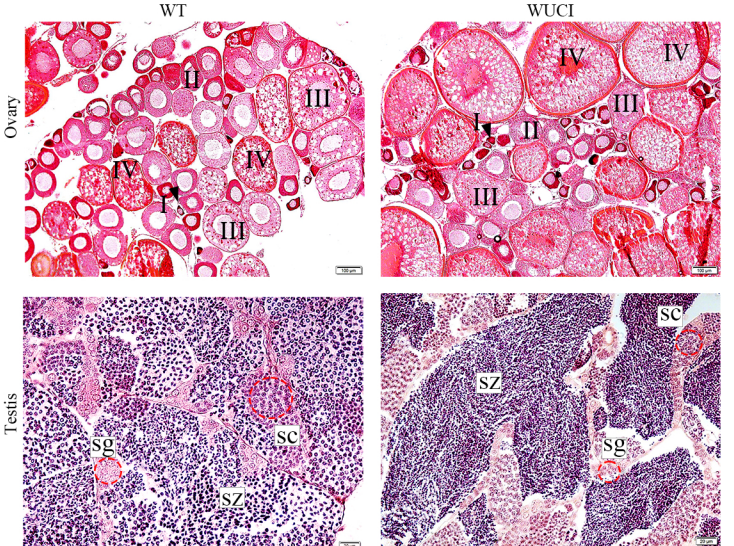
WT
WUCI
Ovary
I
II
III
IV
Testis
SZ
SC
SG
(e)

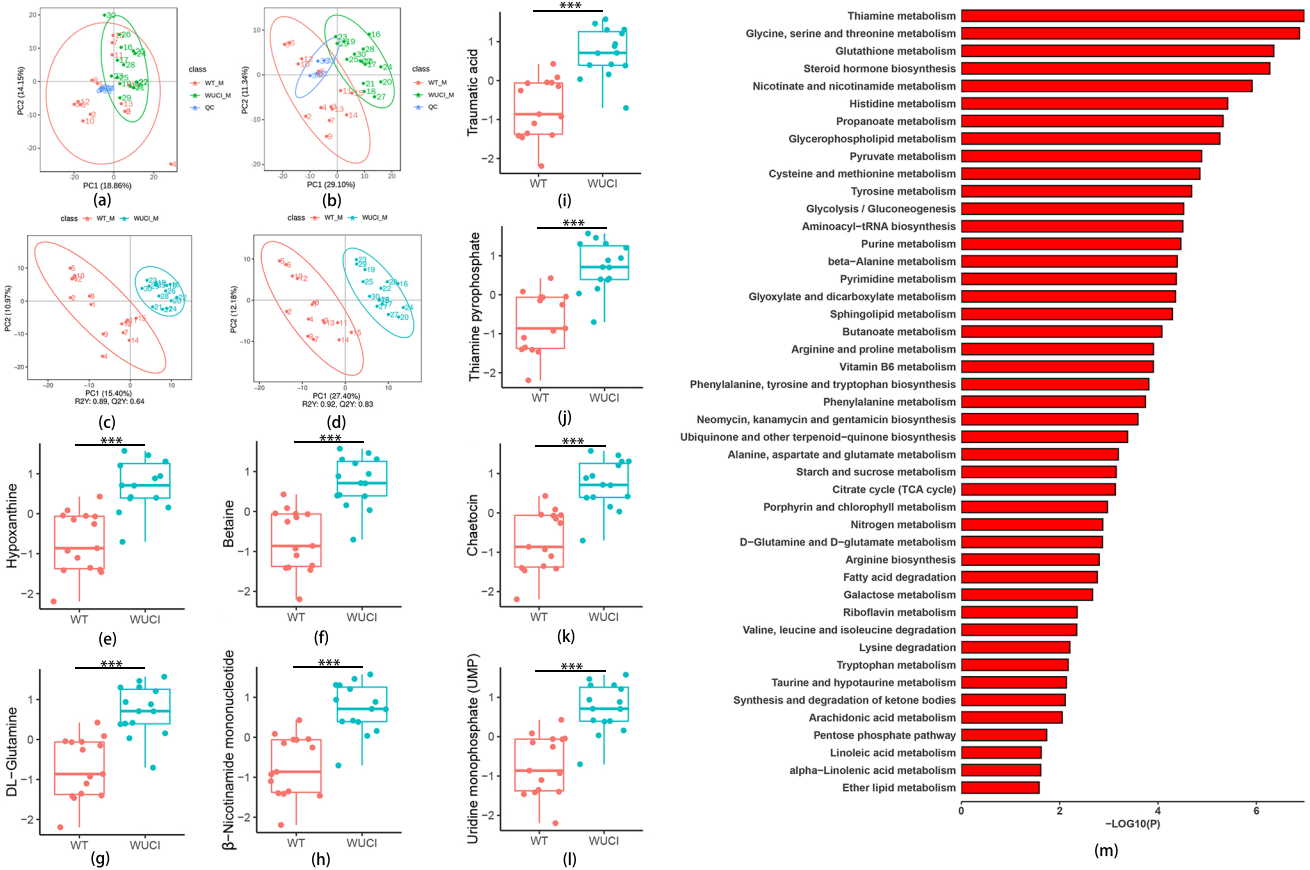
PC1 (18.86%)
PC2 (14.15%)
class
WT_M
WUCI_M
QC
(a)
PC1 (29.10%)
PC2 (11.34%)
(b)
PC1 (15.40%)
PC2 (10.97%)
R2Y: 0.89, Q2Y: 0.64
(c)
PC1 (27.40%)
PC2 (12.18%)
R2Y: 0.92, Q2Y: 0.83
(d)
Hypoxanthine
(e)
Betaine
(f)
DL−Glutamine
(g)
β−Nicotinamide mononucleotide
(h)
Traumatic acid
(i)
Thiamine pyrophosphate
(j)
Chaetocin
(k)
Uridine monophosphate (UMP)
(l)
***
WT
WUCI
Thiamine metabolism
Glycine, serine and threonine metabolism
Glutathione metabolism
Steroid hormone biosynthesis
Nicotinate and nicotinamide metabolism
Histidine metabolism
Propanoate metabolism
Glycerophospholipid metabolism
Pyruvate metabolism
Cysteine and methionine metabolism
Tyrosine metabolism
Glycolysis / Gluconeogenesis
Aminoacyl−tRNA biosynthesis
Purine metabolism
beta−Alanine metabolism
Pyrimidine metabolism
Glyoxylate and dicarboxylate metabolism
Sphingolipid metabolism
Butanoate metabolism
Arginine and proline metabolism
Vitamin B6 metabolism
Phenylalanine, tyrosine and tryptophan biosynthesis
Phenylalanine metabolism
Neomycin, kanamycin and gentamicin biosynthesis
Ubiquinone and other terpenoid−quinone biosynthesis
Alanine, aspartate and glutamate metabolism
Starch and sucrose metabolism
Citrate cycle (TCA cycle)
Porphyrin and chlorophyll metabolism
Nitrogen metabolism
D−Glutamine and D−glutamate metabolism
Arginine biosynthesis
Fatty acid degradation
Galactose metabolism
Riboflavin metabolism
Valine, leucine and isoleucine degradation
Lysine degradation
Tryptophan metabolism
Taurine and hypotaurine metabolism
Synthesis and degradation of ketone bodies
Arachidonic acid metabolism
Pentose phosphate pathway
Linoleic acid metabolism
alpha−Linolenic acid metabolism
Ether lipid metabolism
−LOG10(P)
(m)